ChemEngineering

*Review*

# Artificial Intelligence-Based Models for Wax Deposition Prediction in Oil Pipelines: Potential, Challenges, and Future Directions

**Yaman Hamed [1,*], Omar Nashed [2,*], Eng Hao Louis Tan [1], Engin Sansarcı [3], Petrus Tri Bhaskoro [4], Emad A. Elsebakhi [4] and Md Sohrab Hossain [5]**

[1] Centre for Research in Data Science (CERDAS), Department of Applied Sciences, Universiti Teknologi PETRONAS, Bandar Seri Iskandar 32610, Perak, Malaysia
[2] Faculty of Basic Science, Maaref University of Applied Science, Sarmada, Syria
[3] Department of Industrial Engineering, School of Engineering and Natural Sciences, Istanbul Medipol University, Beykoz, Istanbul 34810, Turkey
[4] Facilities of Future, PETRONAS Research Sdn. Bhd (PRSB), Bangi 43000, Selangor, Malaysia
[5] HICoE-Centre for Biofuel and Biochemical Research, Department of Applied Science, Universiti Teknologi PETRONAS, Bandar Seri Iskandar 32610, Perak, Malaysia
* Correspondence: yaman.hamed@utp.edu.my (Y.H.); onashed86@gmail.com (O.N.)

## Abstract

Wax deposition in pipelines is a major issue in the oil and gas industry. Estimating the main characteristics of the wax deposits is crucial in mitigating their negative impact. Thus, developing predictive models plays an important role in managing wax deposition. Artificial intelligence (AI)-based models have proven their effectiveness and accuracy, along with several advantages such as ease of use, flexibility, and adaptability. This paper presents a comprehensive review of 41 primary studies reporting over 100 individual AI-based models used for wax deposition prediction, including support vector machines (SVMs), feedforward neural networks (multilayer perceptron, RBFNN, cascade-forward, and others), neuro-fuzzy systems, and tree-based models, together with hybrid and metaheuristic-optimized variants. In addition, AI-based models that integrate multiple single-model predictors or optimization techniques were also reviewed. This paper discusses the underlying principles, applications, strengths, and limitations of these AI-based prediction techniques and concludes with an outlook on future research directions in AI-driven wax deposition prediction. According to the reviewed papers, and by analyzing the errors reported, AI-based models can successfully predict the wax deposition rate, deposited weight, thickness, wax appearance temperature (WAT), and wax disappearance temperature (WDT). AI-based models have high potential to compete with conventional models and efficiently contribute to wax deposition control and management. This review finds that although these models routinely report high accuracy ($R^2 > 0.95$), such results are typically obtained on small, frequently reused datasets with limited validation. While gradient-boosting tree ensembles are the most frequent winners in recent head-to-head comparisons, no single model family is consistently superior across prediction targets.

**Keywords:** wax deposition; wax appearance temperature; wax thickness; artificial intelligence; multilayer perceptron; machine learning

Check for updates

Academic Editor: Rajinder Pal

Received: 28 July 2026
Revised: 5 September 2026
Accepted: 15 September 2026
Published: 20 September 2026

**Copyright:** © 2026 by the authors. Licensee MDPI, Basel, Switzerland. This article is an open access article distributed under the terms and conditions of the Creative Commons Attribution (CC BY) license.

## 1. Introduction

Crude oil is a complex mixture of hydrocarbons that vary in composition and molecular structure. In addition to hydrocarbons, it contains other elements such as sulfur, nitrogen, oxygen, and trace amounts of metal compounds. When crude oil has a high concentration of long-chain paraffin waxes, including both normal (n-alkanes) and iso-alkanes, along with aromatics, cycloalkanes, resins, and asphaltenes, it is classified as waxy crude oil [1]. These high-molecular-weight paraffinic compounds, which have a high number of carbon atoms from 18 to 75, are characterized by their high boiling point and ability to deposit as solid wax crystals [2,3]. High-molecular-weight compounds in crude oil remain dissolved under reservoir pressure and temperature conditions. However, during extraction and transportation, the temperature drops and may reach the wax appearance temperature (WAT), defined as the temperature at which the first wax crystals precipitate out of the liquid phase [4]. Wax in crude oil can be broadly classified into two main types: macrocrystalline wax and microcrystalline wax. Macrocrystalline wax consists primarily of straight-chain alkanes (n-alkanes) that form large, needle-like crystals. These waxes tend to precipitate out of the oil during cooling, often leading to flow-assurance issues during production and transportation. In contrast, microcrystalline wax is composed mainly of branched (iso-alkanes) and cyclic hydrocarbons (cycloalkanes). Due to their fine, amorphous crystalline structure, microcrystalline waxes are less prone to forming large crystals but can accumulate as sludge deposits in storage tanks [2]. By cooling below WAT, a layer of gel-like wax deposits is formed on the inner wall of a crude oil pipeline. This deposit is composed of wax crystals as a framework, with liquid oil inside. The formed deposit may cause total pipeline blockage or partial flow restrictions due to the reduction in the inner diameter of the pipeline; subsequently, higher pumping pressures to maintain the flow rate are required. Moreover, this blockage could lead to elevated pressure that may pose significant safety and environmental risks. In addition, equipment such as valves and pumps is susceptible to malfunction or damage due to clogging or the jamming of moving components by wax deposits. The presence of trapped water and other corrosive substances can further accelerate the corrosion of production facilities. Managing wax deposition also presents operational challenges, often requiring mechanical removal methods such as scrapers or pigs, as well as thermal treatments or chemical injection of wax inhibitors. Collectively, these issues significantly increase production costs and contribute to revenue losses due to reduced operational efficiency and downtime [5,6]. Therefore, wax deposition is considered a major issue in flow assurance, especially in offshore operations [2]. However, the depletion of conventional oil wells and the increasing oil demand pose a need to deal with waxy crude oil, while paying considerable attention to ensure safety and economic efficiency.

Several methods are applied to manage and control the wax deposition, including physical and chemical methods. Chemical methods are more feasible in practice [7]. The chemicals added to the oil work by modifying the crystallization process of waxes, reducing the viscosity, altering their morphology, or preventing them from sticking to surfaces [4,7]. These chemicals could be organic material, polymer-based material, or surfactants. These chemicals are categorized based on their function into crystal modifiers, pour point depressants (PPDs), dispersants, and solvents [2,8,9].

In order to manage, predict, and mitigate the wax issues, understanding the mechanism of wax deposition is important. The researchers have made several attempts to propose the wax deposition mechanism. The most common mechanism that has been adopted by many scientists is molecular diffusion [10–14]. This mechanism is a result of the concentration gradient due to the temperature gradient between the pipeline wall and the flowing oil. Another mechanism proposed is Brownian diffusion, which refers to the

random movement of the small wax crystals suspended in the oil [11,15]. Another mechanism, called shear dispersion, was proposed based on the velocity gradient. Additionally, the gravity settling mechanism was proposed to justify wax deposition in a straight pipe under stagnant conditions or at low flow velocities.

It is important to note that wax formation typically occurs in two stages: nucleation followed by growth. The stage of nucleation begins when the fluid temperature approaches WAT. Then, the wax molecules form clusters, and they attach and detach until they reach a critical size where the clusters are stable, called nuclei. Then, the crystal growth stage begins as further molecules attach in a plate-like or lamellar structure [2,16]. When wax is deposited on the inner wall of the pipes, the wax thickness must be monitored to determine the appropriate time to intervene and prevent further operational issues. The techniques used to assess wax thickness can be classified into direct and indirect measurements. Examples of direct measurements include pigging, caliper tools, and spool piece removal [17–19]. For indirect measurement, some variables are measured, followed by calculations and interpretation to determine the thickness. These include pressure drop measurement, ultrasonic techniques, microwave, gamma-ray or X-ray transmission, or external temperature measurement [15,20]. The choice of technique depends on factors such as the required accuracy, the cost, and the disruption to pipeline operation. Direct measurement techniques are generally more accurate but tend to be more disruptive, whereas indirect techniques cause less disruption but may compromise on accuracy [21].

Additionally, it is crucial to monitor the thickness of wax as it begins to accumulate on the pipeline wall. If it becomes a very thick and solid layer, the pig may not be an effective tool due to the possibility of it getting stuck inside the pipes. On the other hand, regular pigging will result in high production expenses [22]. Following the above, there is an imperative need to accurately predict wax thickness and deposition rates. Scientists are actively investigating the underlying mechanisms to develop kinetic and thermodynamic models that support the design of an effective pigging cycle and ensure safe fluid flow.

One way to mitigate the wax impact is to simulate the wax deposition. However, it is difficult to accurately simulate the deposition along the pipeline walls using proper models. This is because the deposition of wax is a result of thermodynamic factors, heat and mass transfer, hydrodynamic flow, as well as solid–solid and surface–solid interactions [23–27]. In addition, modeling will become considerably complicated in the case of multiphase flow because of numerous factors that must be considered.

Therefore, the researchers employed artificial intelligence and data-driven models to predict the WAT, wax disappearance temperature (WDT), wax deposition rate, and wax thickness. Intelligent models exhibit many advantages such as accuracy, adaptability to novel input–output scenarios, ability to model complex nonlinear relationships, suitability for real-time applications, ability to deal with incomplete or noisy data, easy integration and analysis of data from multiple sources, speed, and scalability.

Several AI-based models were employed for wax deposition assessment. The accuracy of prediction depends on the selected model, optimization process, and the input data used. In such data-driven models, the influencing factors are crucial to get precise predictions, as they are the input to the trained system. This review focuses specifically on AI-based prediction of wax deposition in pipeline systems, using a systematic, structured search and a quantitative comparison of reported performance across the different model families. It summarizes the underlying theories and operational principles of major approaches, including machine learning and hybrid intelligent techniques. Key findings from recent studies are compared to highlight performance trends, accuracy, and limitations.

## 2. Review Methodology

### 2.1. Protocol and Reporting

This review was conducted and reported in accordance with the Preferred Reporting Items for Systematic Reviews and Meta-Analyses (PRISMA 2020) guidelines. The objective was to identify primary studies that apply artificial intelligence and machine learning models to the prediction of wax-related outputs in crude oil and condensate systems and to extract their reported model architectures, datasets, input/output variables, and predictive-performance metrics for comparative synthesis.

### 2.2. Information Sources and Search Strategy

Two open bibliographic databases, OpenAlex and Semantic Scholar, were searched as the primary information sources. These were selected because they expose reproducible programmatic Boolean queries and exact result counts, supporting transparent and repeatable searching. Supplementary records were identified through citation chaining and hand-searching of reference lists. Institutional subscriptions to Scopus and Web of Science were not available to the authors. The final search was executed in August 2026 and covered a 20-year window (2006–2026).

The search combined three concept blocks with the Boolean AND operator, with each block being an OR-list of controlled and free-text terms:

(i) Wax target: "wax appearance temperature" OR "wax disappearance temperature" OR WAT OR WDT OR "wax deposition" OR "wax precipitation" OR "wax thickness" OR "wax solubility" OR "paraffin deposition" OR "wax deposit";
(ii) AI/ML method: "machine learning" OR "neural network" OR "support vector" OR "random forest" OR XGBoost OR ANFIS OR "deep learning" OR "data-driven" OR "artificial intelligence" OR "gradient boosting";
(iii) Prediction: predict* OR estimat* OR forecast* OR model*.

### 2.3. Eligibility Criteria

Studies were included if they satisfied all of the following: (1) they were primary studies applying an artificial intelligence or machine learning model, predominantly a regression model, to predict at least one wax-related output (WAT, WDT, wax deposition rate, deposited wax mass or percentage, wax deposition thickness, or wax precipitation/solubility) in crude oil or condensate systems; (2) the model architecture was described in sufficient detail to be identified; (3) at least one quantitative predictive-performance metric was reported (e.g., $R^2$, RMSE, AAPRE, MSE; defined in Section 3.2); (4) the dataset, input variables, and output variable(s) were documented; and (5) the study was published in English between 2006 and 2026.

Studies were excluded if they met any of the following criteria: (1) non-primary works (reviews, editorials, notes); (2) purely thermodynamic, mechanistic, or empirical models with no ML component; (3) classification-only models or models predicting non-wax targets (e.g., asphaltene precipitation, apparent viscosity, shear stress, liquid holdup, or oil-sludge formation); (4) models based on convolutional neural network (CNN) or recurrent neural network (RNN) architectures operating on non-tabular (image or sequence) inputs, as the review targets tabular compositional and operational inputs; (5) no quantitative performance metric reported, or insufficient dataset/architecture detail; and (6) duplicate records.

### 2.4. Study Selection

Records from the two databases were pooled and de-duplicated automatically using a custom Python 3.12 script, first by Digital Object Identifier (DOI) and, for records lacking a DOI, by normalized title. The de-duplicated set was screened at the title-and-abstract

level. To prioritize screening, a keyword filter treated records containing no wax- or paraffin-related term as off-topic; all remaining records were then assessed individually against the eligibility criteria. Records passing title/abstract screening were retrieved in full text and assessed for eligibility. Both screening stages were performed independently by two reviewers, and disagreements were resolved by discussion or, where necessary, by consulting the primary source.

### 2.5. Data Extraction

For each included study, the following items were extracted into a structured dataset: bibliographic details; model family and specific architecture, including any optimizer or hybridization; prediction target; input variables; dataset size (number of data points); data source; and all reported predictive-performance metrics. Where a study reported multiple models, each was recorded as a separate entry, so that a single study could contribute several model instances to the dataset. Reported metrics were standardized to three decimal places, and held-out test values were used where both training and test performance were reported. Correlation coefficients were recorded as such and not treated as coefficients of determination. Studies whose dataset size was inflated by simulation or data augmentation were flagged and excluded from dataset-size analyses.

A formal risk-of-bias instrument was not applied; instead, minimum methodological adequacy was enforced through the eligibility criteria, which required an identifiable architecture, a documented dataset and variables, and at least one quantitative performance metric. Because the extracted metrics span different prediction targets, units, datasets, and validation protocols, a formal meta-analysis was not appropriate. Results were therefore synthesized narratively, with extracted metrics stratified by prediction target to support valid comparison.

### 2.6. Selection Outcome

The database searches returned 429 records (227 from OpenAlex and 202 from Semantic Scholar). After the removal of 153 duplicates, 276 unique records were screened by title and abstract, of which 179 were excluded as off-topic. Of the 97 reports sought for retrieval, 17 could not be retrieved. The remaining 80 reports were assessed for eligibility in full text, and 40 were excluded with reasons: no quantitative performance metrics reported (15); non-wax-prediction target (9); non-primary/review (6); convolutional or recurrent architecture on non-tabular inputs (4); classification-only model (4); thesis lacking a corresponding peer-reviewed publication (1); and duplicate record not resolved by automated de-duplication (1). This yielded 40 studies from database searching. One further study meeting all eligibility criteria was identified through hand-searching, giving a total of 41 included studies, which together contributed 105 individual model instances to the extracted dataset. The selection process is summarized in the PRISMA 2020 flow diagram (Figure 1).

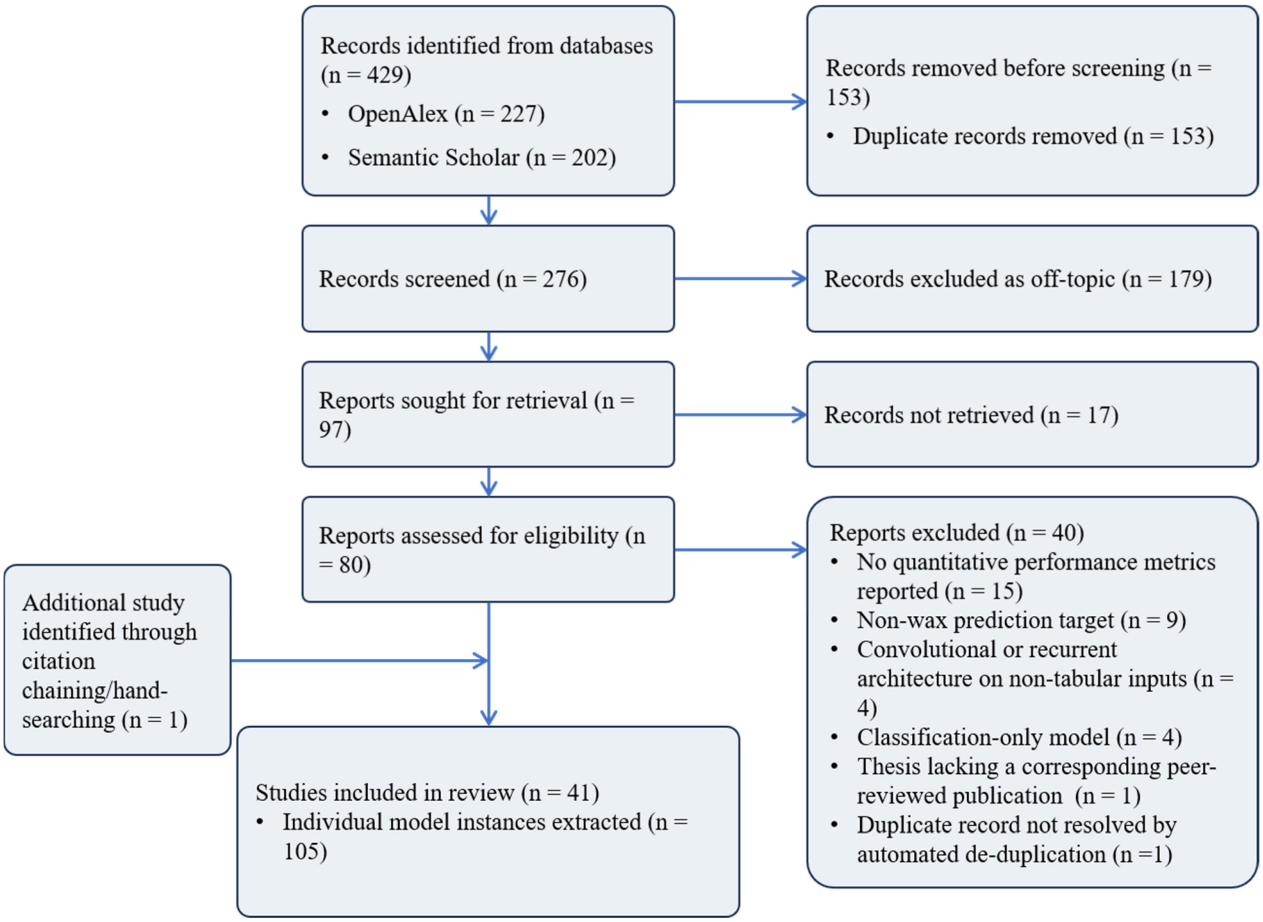


**Figure 1.** PRISMA flow diagram of the study selection process.

## 3. Data-Driven Artificial Intelligence (AI)-Based Modeling

Data-driven models learn the mapping between operational and compositional inputs and wax-related targets directly from data, without explicitly solving the underlying transport and thermodynamic equations. This section describes how such models are built (Section 2.1), how their accuracy is measured (Section 2.2), the architectures applied to wax prediction (Section 2.3), and the algorithms used to train and tune them (Section 2.4).

### *3.1. Model Development Workflow*

AI-based model development proceeds through five stages—data collection, preprocessing, training, validation, and optimization, as summarized in Figure 2 [28–31]. In wax prediction, the inputs are typically temperature, pressure, flow dynamics, crude oil composition (carbon-number fractions), and density, while the targets are the wax appearance temperature (WAT), wax disappearance temperature (WDT), wax deposition rate, or wax thickness (precipitated weight). Data are drawn from laboratory experiments, field measurements, process simulators (e.g., OLGA), or the compiled literature.

Preprocessing places the data on a common scale. Normalization is the most common step; it speeds convergence and prevents large-range features from dominating [29,31]. Two schemes are commonly used: min–max scaling to [0, 1] (Equation (1)), preferred for non-negative or distance-based models, and symmetric scaling to [−1, 1] (Equation (2)), preferred where zero-symmetry helps (SVM, regression, and ANN models) [32–35].

$$X_{norm} = \frac{X - X_{min}}{X_{max} - X_{min}} \quad (1)$$

$$X_{norm} = 2 \cdot \frac{X - X_{min}}{X_{max} - X_{min}} - 1 \quad (2)$$

Here, $X_{norm}$ is the normalized value, $X$ is the original value, and $X_{min}$ and $X_{max}$ are the dataset minimum and maximum values.

During training, an optimization algorithm (Section 2.4) iteratively updates the model parameters to minimize the prediction error; regularization can be added to limit overfitting. Validation then evaluates the trained model on a held-out test set to confirm that it generalizes rather than memorizes: a large gap between training and test accuracy signals overfitting and prompts remedies such as reduced model complexity, more data, or cross-validation [29,31]. Finally, optimization tunes the hyperparameters of the machine learning model to balance training accuracy against generalization [36].

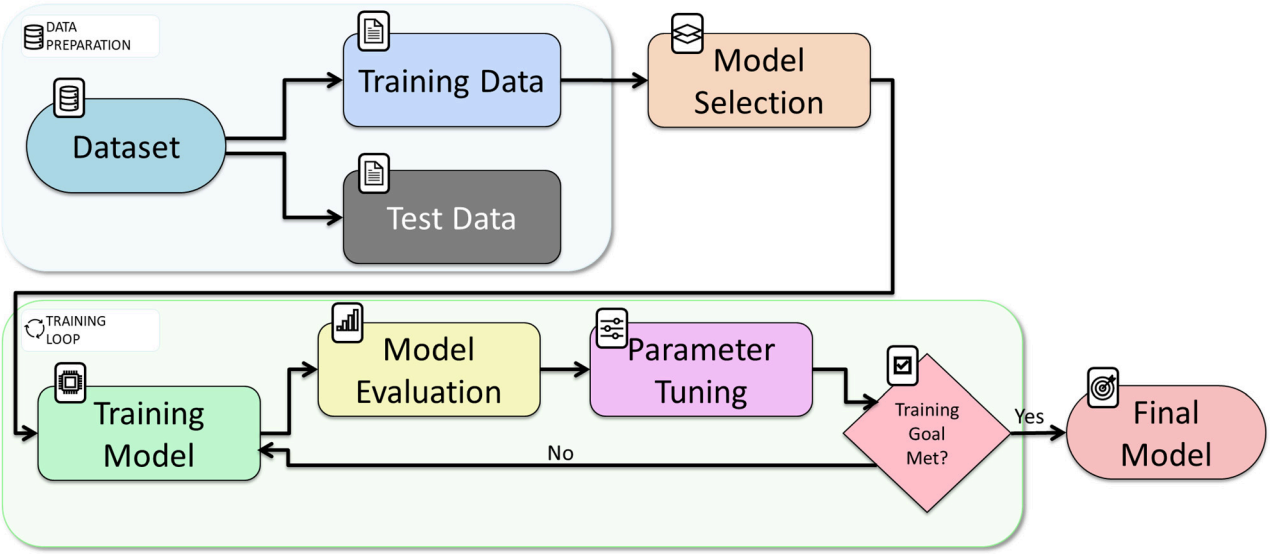


**Figure 2.** Systematic workflow for artificial intelligence (AI)-based model development.

### *3.2. Evaluation Metrics*

Accuracy across the reviewed literature is reported with four metrics. The coefficient of determination ($R^2$, Equation (3)) measures the explained variance, with values near 1 indicating a better fit. The mean-squared error (MSE, Equation (4)) and root-mean-squared error (RMSE, Equation (5)) measure absolute error, with lower values preferred. The average absolute percent relative error (AAPRE, Equation (6)) measures the mean relative error as a percentage. It also appears under the aliases average absolute relative deviation (AARD) and mean absolute percentage error (MAPE).

$$R^2 = 1 - \frac{\sum_{i=1}^{n}\left(X^i_{pred.} - X^i_{exp.}\right)^2}{\sum_{i=1}^{n}\left(X^i_{exp.} - \overline{X}_{exp}\right)^2} \quad (3)$$

$$MSE = \frac{\sum_{i=1}^{n}\left(X^i_{pred.} - X^i_{exp.}\right)^2}{n} \quad (4)$$

$$RMSE = \sqrt{\frac{\sum_{i=1}^{n}\left(X^i_{pred.} - X^i_{exp.}\right)^2}{n}} \quad (5)$$

$$AAPRE = \frac{100}{n} \times \sum_{i=1}^{n}\left|\frac{X^i_{exp.} - X^i_{pred.}}{X^i_{exp.}}\right| \quad (6)$$

Here, $n$ is the number of data points; $X^i_{pred.}$ and $X^i_{exp.}$ are the $i$-th predicted and experimental values; and $\overline{X}_{exp}$ is the mean of the experimental values.

### 3.3. Model Architectures Applied for Wax Prediction

The architectures applied to wax prediction fall into five families: support vector machines (SVMs), feedforward neural networks, neuro-fuzzy systems, tree-based models, and others. Figure 3 shows this categorization. Their formulations and trade-offs are summarized in Table 1.

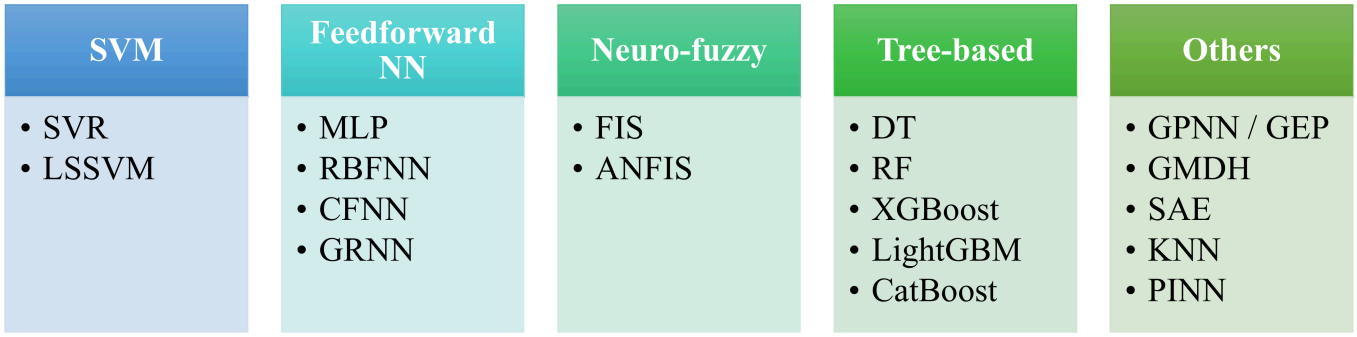


**Figure 3.** Categorization of machine learning models used for wax deposition prediction.

**Table 1.** Architectures applied to wax deposition prediction.

| Family | Model | Core Formulation/Idea | Strengths | Limitations |
|---|---|---|---|---|
| SVM | SVR | $y = f(x) = w \cdot \phi(x) + b$ <br> $\min_{w,b,\xi,\xi^*} \frac{1}{2}\|\|w\|\|^2 + C\sum_{i=1}^{n}(\xi_i + \xi_i^*)$ | Robust on small noisy data; RBF kernel best | Kernel/hyperparameter sensitivity |
| SVM | LSSVM | $y = f(x) = w \cdot \phi(x) + b + e_i, i = 1, 2, \ldots, n$ <br> $\begin{bmatrix} 0 & 1^T \\ 1 & \Omega + \frac{I}{\gamma} \end{bmatrix} \begin{bmatrix} b \\ \alpha \end{bmatrix} = \begin{bmatrix} 0 \\ y \end{bmatrix}$ | Fast, fewer hyperparameters | Loses sparsity of SVR |
| Feedforward NN | MLP | $a_j^{(l)} = \sigma\left(\sum_{i=1}^{n^{(l-1)}} w_{ij}^{(l)} a_i^{(l-1)} + b_j^{(l)}\right)$ | Universal approximator | Needs care vs. overfitting on tiny sets |
| | RBFNN | $\phi_j(X) = exp\left(-\frac{\|\|X-c_j\|\|^2}{2\sigma_j^2}\right)$ | Fast local approximation | Spread/center sensitivity; scales poorly |
| | CFNN/GRNN | Direct skip connections/single-pass kernel regression | Quick, little/no training (GRNN) | Mostly comparison baselines |
| Neuro-fuzzy | FIS/ANFIS | TSK fuzzy rule: $f_i = p_i\, x + q_i\, y + r_i$ | Interpretable; handles imprecision | Rule explosion with many inputs |
| Tree-based | DT | Recursive feature-space splits; piecewise-constant leaves | Interpretable; no feature scaling | Unstable; overfits when used alone |
| | RF | Bagged ensemble of de-correlated trees; outputs averaged | Robust; lowers single-tree variance | Less interpretable; weak extrapolation |
| | XGBoost/LightGBM/ CatBoost | Gradient-boosted additive trees with regularization | Strongest on small tabular wax data | Tuning-heavy; cannot extrapolate |
| Others | GPNN/GEP | Genetic-programming search over network/expression structure | Evolves model structure automatically | Computationally costly; stochastic results |
| | GMDH | Self-organizing polynomial network; layer-wise node selection | Explicit equations; automatic structure | Polynomial term growth; overfitting risk |
| | KNN | Instance-based prediction from the $k$ nearest samples using a distance metric | Simple; non-parametric; captures local nonlinear trends | Sensitive to feature scaling and choice of $k$; weak extrapolation |

**Table 1.** *Cont.*

| Family | Model | Core Formulation/Idea | Strengths | Limitations |
|---|---|---|---|---|
| | SAE | Unsupervised layer-wise pretraining + supervised fine-tuning | Learns features from large datasets | Data-hungry; needs large sets |
| | PINN | Embeds governing physics as a loss regularizer | Aids extrapolation; physically consistent | Prior–data balance can bias the fit |

Note. Throughout, subscripts index individual neurons, basis functions, or fuzzy rules; a superscript (l) denotes the l-th network layer; and a superscript T denotes the transpose. Symbols: $x$, input feature vector; $X$, input vector (RBFNN); $y$, model output (target); $f(x)$, prediction function; $w$, weight vector; $b$, bias term; $\varphi(\cdot)$, nonlinear feature-space (kernel) mapping; $\xi$ and $\xi^*$, slack variables of the $\varepsilon$-insensitive loss; $C$, SVR penalty parameter; $e$, LSSVM regression error; $\gamma$, LSSVM regularization parameter; $\Omega$, kernel (Gram) matrix; $I$, identity matrix; 1, column vector of ones; $\alpha$, support-value (Lagrange-multiplier) vector; $a$, neuron activation; $\sigma(\cdot)$, activation function; $n$, number of neurons in a layer; $c$, basis function center; $\sigma$ (subscripted), basis function width; $p$, $q$ and $r$, consequent parameters of a Takagi–Sugeno rule; $\|\cdot\|$, Euclidean norm. Abbreviations: SVM, support vector machine; SVR, support vector regression; LSSVM, least-squares support vector machine; MLP, multilayer perceptron; RBF, radial basis function; RBFNN, radial basis function neural network; CFNN, cascade-forward neural network; GRNN, generalized regression neural network; FIS, fuzzy inference system; ANFIS, adaptive neuro-fuzzy inference system; DT, decision tree; RF, random forest; XGBoost, extreme gradient boosting; LightGBM, light gradient-boosting machine; CatBoost: Categorical Boosting; GPNN, genetic-programming neural network; GEP, gene expression programming; GMDH, group method of data handling; KNN: K-nearest neighbors; SAE, stacked auto-encoder; PINN, physics-informed neural network; NAS, neural architecture search; SHAP, Shapley additive explanations; UQ, uncertainty quantification.

SVMs fit a function within an $\varepsilon$-insensitive margin and use kernels to map inputs into a higher-dimensional space [37–39]. Support vector regression (SVR) is the regression form used for wax prediction. The least-squares SVM (LSSVM) replaces SVR's inequality constraints with equality constraints and a squared-error term, reducing the problem to a linear system with fewer hyperparameters [40,41]. This lowers computational cost but sacrifices the sparsity of the standard SVM, since every training point contributes to the model. SVMs are common in wax work because the datasets are small and noisy, conditions under which margin-based regularization controls overfitting. The radial basis function (RBF) kernel is the best-performing kernel in the surveyed SVM/LSSVM studies.

Feedforward neural networks dominate the field. The multilayer perceptron (MLP) is the most common model. It is a universal approximator, trained by backpropagation, that handles the small-to-moderate tabular regression typical of wax data with minimal architecture search. However, it requires careful regularization and early stopping to avoid overfitting on small datasets. Radial basis function neural networks (RBFNNs) use localized Gaussian responses for fast training and good local approximation, but are sensitive to spread and center selection and scale poorly with input dimensionality. Cascade-forward neural networks (CFNNs), which add direct connections from each layer to all later layers, and generalized regression neural networks (GRNNs), which apply kernel regression without iterative training, appear mainly as comparison baselines [42,43].

Neuro-fuzzy systems encode if–then rules with fuzzy membership functions. Fuzzy inference systems (FISs) process information through degrees of membership rather than binary truth values, capturing uncertainty and imprecision [44,45]. The adaptive neuro-fuzzy inference system (ANFIS), introduced by Jang in 1993, overlays neural network learning onto a Takagi–Sugeno rule base, combining interpretability and adaptability with a rule count that grows combinatorially with input dimensions [46–48].

Tree-based models partition the feature space into regions and fit a simple prediction within each. The decision tree (DT) recursively splits the data through a root node, decision nodes, and leaf nodes, with each split chosen to minimize the prediction error (typically MSE) [29]. A single DT is interpretable but unstable, as small data changes can alter its

structure. Ensembles overcome this by combining many trees. Random forests (RFs) and extremely randomized trees (extra-trees, ET) average de-correlated trees trained on bootstrap or randomized splits to reduce variance. Gradient-boosting methods such as XGBoost and LightGBM build trees sequentially and currently rank among the strongest performers on small tabular wax datasets, while CatBoost uses ordered boosting to improve generalization and efficiently handle categorical features.

Several architectures appear less frequently. Committee machines (CMs) combine parallel models, merging their outputs by averaging, voting, or weighting to improve robustness [31]. The group method of data handling (GMDH) is a polynomial neural network that builds explicit input–output relations through layers of polynomial nodes. Genetic-programming approaches like the genetic-programming neural network (GPNN) and gene expression programming (GEP) evolve the model structure itself, with GPNN evolving the network topology and GEP yielding explicit symbolic equations. The stacked auto-encoder (SAE) performs unsupervised, layer-wise feature pretraining and is justified mainly for large, often simulator-generated datasets. K-nearest neighbors (KNN) is a non-parametric, instance-based method that predicts an output from the values of the k most similar training samples, making its performance sensitive to feature scaling and the choice of k. The physics-informed neural network (PINN), the newest entrant, embeds governing physical relations into the loss as a regularizer. The Elman neural network (ENN) also appears sporadically.

### *3.4. AI-Based Model Training and Optimization Strategies*

Training algorithms fall into two classes, shown in Figure 4 and detailed in Table 2. Namely, (1) gradient-based methods, which use derivatives of the loss to descend the error surface, and (2) gradient-free metaheuristics, which search the solution space through population-based heuristics and are valuable where the objective is non-differentiable or rich in local optima.

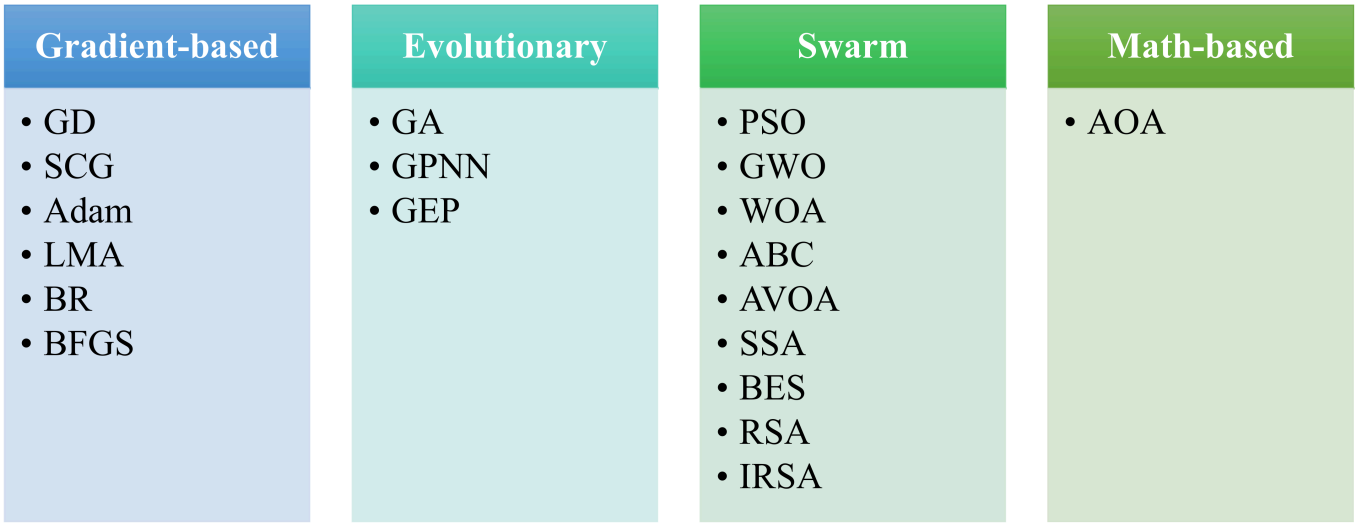


**Figure 4.** Categorization of optimization algorithms used to train AI models for wax deposition prediction.

Among the gradient-based methods, plain gradient descent and its scaled conjugate gradient (SCG) and adaptive-moment (Adam) variants are first-order schemes. The Levenberg–Marquardt algorithm (LMA) and BFGS are second-order or quasi-Newton schemes that converge faster on the small networks typical of wax models. LMA is the most common MLP trainer. Bayesian regularization (BR) adds a weight penalty to the objective to curb overfitting and is the usual benchmark against LMA.

**Table 2.** Optimization algorithms used in wax-prediction studies.

| Algorithm | Class | Core Formulation/Idea | Strengths | Role in Wax Modeling |
|---|---|---|---|---|
| Gradient Descent | First-order | $\theta^{(t+1)} = \theta^{(t)} - \eta \nabla L\left(\theta^{(t)}\right)$ | Simple, scalable | Baseline trainer |
| SCG | Conjugate gradient | Conjugate directions + adaptive step; auto learning rate | No line search; automatic step size | Stable; fewer hyperparameters |
| Adam | First-order (adaptive) | Adaptive first/second moment estimates of the gradient | Fast, robust default | Common deep-network trainer |
| LMA | Second-order (damped Gauss–Newton) | $\theta^{(t+1)} = \theta^{(t)} - \left(J^T J + \lambda I\right)^{-1} J^T e$ | Fast convergence on small networks | Most common MLP trainer |
| Bayesian Regularization | Gradient + penalty Weight Penalty | $L(\theta) = \alpha E_D + \beta E_W$ | Auto-regularization; no separate validation set | Curbs overfitting, point estimates, not UQ |
| BFGS | Quasi-Newton | Iterative inverse-Hessian approximation | Superlinear convergence | Emerging; may outperform LMA |
| GA | Evolutionary | Selection/crossover/mutation | Global, gradient-free search | Tunes weights, architecture |
| GPNN | Evolutionary (GP) | Evolves network topology (NAS) | Automates network topology | Architecture search |
| GEP | Evolutionary (GP) | Evolves explicit expressions (genotype/phenotype split) | Yields explicit symbolic models | Symbolic model discovery |
| ABC | Swarm | Honeybee foraging (employed/onlooker/scout) | Few control parameters | Hybrid NN/RBFNN tuning |
| PSO | Swarm | Bird flock; personal + global best | Simple; fast convergence | Common ANFIS optimizer |
| GWO | Swarm | Gray wolf hierarchy ($\alpha/\beta/\delta/\omega$) | Few parameters; good balance | Balanced exploration/exploitation |
| WOA | Swarm | Humpback bubble-net hunting | Simple; strong exploration | NN weight/parameter tuning |
| AVOA | Swarm | African vulture foraging behavior | Strong exploration; SHAP-paired | Optimizes BP NN; interpretable |
| AOA | Math-based | Arithmetic operators | Low-cost arithmetic operators | Optimizes Elman NN |
| RSA | Swarm | Reptile search | Strong exploration | Baseline for IRSA |
| IRSA | Swarm | Improved reptile search + chaotic map | Chaotic map improves search | Optimizes Elman NN |
| SSA | Swarm | Sparrow search | Fast; good convergence | Optimizes BP NN (cold-region data) |
| BES | Swarm | Bald eagle search (+gray relational analysis) | Balanced search; few parameters | Optimizes BP NN (diesel wax) |

Note. Throughout, $\theta$ denotes the trainable parameters (network weights) and a superscript (t) is the iteration index. Symbols: $\eta$, learning rate; $\nabla$, gradient operator; $L$, loss (objective) function; $E_D$ and $E_W$, the data-error and weight-penalty terms of the Bayesian objective; $\alpha$ and $\beta$, their associated regularization hyperparameters; $J$, Jacobian of the residuals (Levenberg–Marquardt); $\lambda$, Levenberg–Marquardt damping parameter; $I$, identity matrix; $e$, residual (error) vector. Within the gray wolf operator, $\alpha$, $\beta$, $\delta$ and $\omega$ denote the wolf-rank hierarchy rather than numerical parameters. Abbreviations: GD, gradient descent; SCG, scaled conjugate gradient; Adam, adaptive-moment estimation; LMA, Levenberg–Marquardt algorithm; BR, Bayesian regularization; BFGS, Broyden–Fletcher–Goldfarb–Shanno; GA, genetic algorithm; GP, genetic programming; GPNN, genetic-programming neural network; GEP, gene expression programming; ABC, artificial bee colony; PSO, particle swarm optimization; GWO, gray wolf optimizer; WOA, whale optimization algorithm; AVOA, African vulture optimization algorithm; AOA, arithmetic optimization algorithm; RSA, reptile search algorithm; IRSA, improved reptile search algorithm; SSA, sparrow search algorithm; BES, bald eagle search; NN, neural network; BP, backpropagation; ENN, Elman neural network; NAS, neural architecture search; SHAP, Shapley additive explanations; UQ, uncertainty quantification.

The metaheuristics divide into evolutionary, swarm, and math-based families. Evolutionary methods (the genetic algorithm (GA), GPNN, and GEP) evolve solutions through selection, crossover, and mutation. Swarm methods, including particle swarm optimization (PSO), gray wolf optimizer (GWO), whale optimization algorithm (WOA), artificial bee colony (ABC), African vulture optimization (AVOA), sparrow search (SSA), bald eagle search (BES), and reptile search (RSA/IRSA), emulate collective animal behavior. The arithmetic optimization algorithm (AOA) is math-based. In the wax literature, these metaheuristics serve almost exclusively as weight or hyperparameter optimizers wrapped around MLP and ANFIS, with the aim of escaping local minima and avoiding manual tuning.

## 4. Applied AI-Based Models in Wax Deposition Prediction

This section reviews the reported AI-based wax-prediction models, grouped by the five families of Section 2.3. Each study's dataset, architecture, target, and test-set accuracy ($R^2$, RMSE, AAPRE) are summarized in Table 3, Table 4, Table 5, Table 6, and Table 7, respectively. Where a study compared models from different families, its result is reported under each relevant subsection. Figure 5 traces when each family was adopted. Feedforward networks and SVMs span the entire period, neuro-fuzzy systems cluster in the mid-2010s, and tree-based models appear only in the most recent studies.

**Table 3.** Summary of SVM-based models used for wax deposition prediction (unless noted, $R^2$, AAPRE, and RMSE are test-set values).

| Reference | Data Source (Size) | Input Parameters | Target | Architecture and Optimization | Summary of Results |
|---|---|---|---|---|---|
| Kamari et al. (2013) [49] | Pedersen et al. (1991) [50]; 87 pts | $C_1$–$C_3$, $C_4$–$C_7$, $C_8$–$C_{15}$, $C_{16}$–$C_{22}$, $C_{23}$–$C_{29}$, $C_{30+}$, specific gravity, pressure, temperature | Wax precipitation weight | LSSVM with radial basis function kernel, C = 615.8804 and $\sigma^2$ = 0.72381 | $R^2$ = 0.989<br>AAPRE = 36.30%<br>RMSE = 0.440 |
| Kamari et al. (2014) [51] | Wei et al. (2010) [52]; 10 pts | Viscosity, wall shear stress, temperature gradient at pipeline wall, wax concentration gradient | Wax deposition rate | LSSVM with radial basis function kernel, $\sigma^2$ = 6.0568, $\gamma$ = 13642 | $R^2$ = 0.999<br>AAPRE = 0.05%<br>RMSE = 0.006 |
| Gholami et al. (2018) [53] | Literature compilation [50,54,55] | $C_1$–$C_3$, $C_4$–$C_7$, $C_8$–$C_{15}$, $C_{16}$–$C_{22}$, $C_{23}$–$C_{29}$, $C_{30+}$, specific gravity, temperature | Wax precipitation weight | SVR with sigmoid kernel function (C, $\epsilon$, Coef, $\gamma$ = 179.1758, 0.007, 0.0673, 0.1918) | $R^2$ = 0.838<br>RMSE = 1.286 |
| | | | | SVR with radial basis function kernel, (C, $\epsilon$, $\gamma$ = 61.1818, 0.0001, 6.6548) | $R^2$ = 0.968<br>RMSE = 0.570 |
| | | | | SVR with linear kernel function (C, $\epsilon$ = 1.3193, 0.1531) | $R^2$ = 0.828<br>RMSE = 1.325 |
| Bian et al. (2019) [56] | Literature compilation [57–59]; 272 pts | Pressure, molar mass | WDT | SVM-GWO with radial basis function kernel. Maximum 100 iterations, 30 search agents, (C, $\epsilon$, $\gamma$ = 35.1846, 0.0019, 0.2231) | $R^2$ = 0.943<br>AAPRE = 0.69%<br>RMSE = 2.404 |

**Table 3.** *Cont.*

| Reference | Data Source (Size) | Input Parameters | Target | Architecture and Optimization | Summary of Results |
|---|---|---|---|---|---|
| | | | | LSSVM with radial basis function kernel | $R^2$ = 0.946<br>AAPRE = 0.77%<br>RMSE = 2.824 |
| Kamari et al. (2019) [60] | Literature compilation [57–59,61–63]; 254 pts | Pressure, molar mass | WDT | LSSVM with radial basis function kernel of C = 2138.4288 and $\sigma^2$ = 40.8325 | $R^2$ = 0.950<br>AAPRE = 0.60%<br>RMSE = 2.200 |
| Septiano et al. (2022) [64] | Literature compilation [52,65,66]; 75 points, augmented to 13,995 simulated | Water volume fraction, wall shear stress, dynamic viscosity, temperature gradient at pipeline wall, wax concentration gradient | Wax deposition rate | SVR, (C,$\epsilon$ = 2.05, 0.10) | $R^2$ = 0.945<br>RMSE = 0.493 |
| Khalighi and Cheremisin (2024) [67] | Pedersen et al. (1991) [50]; 87 pts | $C_1$–$C_3$, $C_4$–$C_7$, $C_8$–$C_{15}$, $C_{16}$–$C_{22}$, $C_{23}$–$C_{29}$, $C_{30+}$, Specific gravity, temperature | Wax precipitation weight | LSSVM-GA, C = 19.1668 and $\sigma^2$ = 4.8490; 400 iterations, population size of 50, crossover percentage of 0.8, mutation percentage of 0.3 | $R^2$ = 0.939<br>RMSE = 1.113 |
| | | $C_4$–$C_7$, $C_8$–$C_{15}$, $C_{16}$–$C_{22}$, $C_{23}$–$C_{29}$, $C_{30+}$, temperature | Wax precipitation weight | LSSVM-GA, C = 9.91e7 and $\sigma^2$ = 48.8403; 400 iterations, population size of 50, crossover percentage of 0.8, mutation percentage of 0.3 | $R^2$ = 0.988<br>RMSE = 0.360 |
| Kouhi et al. (2025) [68] | Literature compilation [69–71]; 81 pts | Density, wax content, pour point | WAT | LSSVM, with radial basis function kernel ($\gamma$ = 120, $\sigma^2$ = 0.2) | $R^2$ = 0.999<br>AAPRE = 3.41%<br>RMSE = 0.007 |
| Gao et al. (2026) [72] | 85 field samples, Qinghai oilfield pipeline, then augmented to 1060 via WGAN-GP | Temperature, flow velocity, wax content, pressure, viscosity | Wax deposition rate | SVR (C,$\epsilon$,$\gamma$ = 100, 0.1) | $R^2$ = 0.961<br>RMSE = 0.540 |
| Sarkodie et al. (2026) [73] | Literature compilation [66,74,75]; 215 pts | Temperature, wall temperature, viscosity, wall shear stress, flow velocity, temperature gradient at pipeline wall, wax concentration gradient | Wax deposition rate | SVR | $R^2$ = 0.970<br>AAPRE = 12.32%<br>RMSE = 0.144 |

**Table 4.** Summary of feedforward neural network models used for wax deposition prediction (unless noted, $R^2$, AAPRE, and RMSE are test-set values).

| Reference | Data Source (Size) | Input Parameters | Target | Architecture and Optimization | Summary of Results |
|---|---|---|---|---|---|
| Huang and Ma (2008) [76] | Daqing oilfield (field); 26 pts | Viscosity, wall shear stress, temperature gradient at pipeline wall, wax concentration gradient | Wax deposition rate | MLP-LMA of shape 4-4-1 | corr = 0.95 |
| Obanijesu and Omidiora (2008) [77] | 11 Nigerian crude reservoirs (field) | Viscosity | Wax deposition potential | MLP | corr = 0.970 |

**Table 4.** *Cont.*

| Reference | Data Source (Size) | Input Parameters | Target | Architecture and Optimization | Summary of Results |
|---|---|---|---|---|---|
| Wei et al. (2010) [52] | Not reported | Wall shear stress, temperature gradient at pipeline wall, wax concentration gradient, viscosity | Wax deposition rate | MLP of shape 4-7-1 | AAPRE < 2.00% |
| Manshad et al. (2012) [55] | Pedersen et al. (1991) [50]; 87 pts | $C_1$–$C_3$, $C_4$–$C_7$, $C_8$–$C_{15}$, $C_{16}$–$C_{22}$, $C_{23}$–$C_{29}$, $C_{30+}$, specific gravity, pressure, temperature | Wax precipitation weight | MLP-LMA | $R^2$ = 0.983 |
| Kelechukwu et al. (2013) [78] | Own experiments, Malaysian crude; 360 pts | Temperature differential, flow rate, residence time | Wax deposition mass | MLP-LMA of shape 3-12-1 | $R^2$ = 0.983 (Calculated from reported data) |
| Moradi et al. (2013) [79] | Literature compilation [57–59,61–63]; 306 pts | Pressure, molar mass | WDT | MLP-LMA of shape 2-16-1 | $R^2$ = 0.988 AAPRE = 0.49% |
| Behbahani et al. (2015) [80] | Iranian waxy crude (experimental) | Temperature, oil composition, wax content | Wax precipitation/WAT | MLP-LMA of shape 3-4-10-1 | AAPRE < 4.00% |
| Eghtedaei et al. (2017) [81] | Literature compilation [50,54,82] | $C_1$–$C_3$, $C_4$–$C_7$, $C_8$–$C_{15}$, $C_{16}$–$C_{22}$, $C_{23}$–$C_{29}$, $C_{30+}$, Specific gravity, pressure, temperature | Wax precipitation weight | RBFNN-LMA | $R^2$ = 0.998 AAPRE = 11.74% RMSE = 0.171 |
| Saeedi Dehaghani et al. (2017) [83] | Literature compilation [84–86]; 1560 pts | Reynolds number, Residence time, temperature driving force, wax content | Wax deposition thickness | MLP-LM of shape 4-19-8-1 | $R^2$ = 0.999 AAPRE = 4.54% |
| Xie and Xing (2017) [66] | Huachi crude, from Wang 2010 [87]; 38 pts | Temperature gradient at pipeline wall, wax solubility, wall shear stress, viscosity | Wax deposition rate | RBFNN goal of 0.001 and spread of 2 | AAPRE < 1.50% |
| Gholami et al. (2018) [53] | Literature compilation [50,54,55] | $C_1$–$C_3$, $C_4$–$C_7$, $C_8$–$C_{15}$, $C_{16}$–$C_{22}$, $C_{23}$–$C_{29}$, $C_{30+}$, specific gravity, temperature | Wax precipitation weight | MLP-LMA with 6 hidden layer neurons | $R^2$ = 0.972 MSE = 0.300 RMSE = 0.548 |
| Benamara et al. (2019) [88] | Lit. compilation [57–59]; 272 pts | Pressure, molar mass | WDT | RBFNN-ABC of 36 hidden layer neurons, spread = 1.1883. Maximum of 50 iterations, 20 employer bees, 20 onlooker bees, 5 scout bees iterations. | $R^2$ = 0.957 AAPRE = 0.61% RMSE = 2.179 |
| | | | | RBFNN-GA of 32 hidden layer neurons, spread = 0.5392. Maximum of 50 generations, population size of 40, crossover percentage of 0.87, mutation percentage of 0.2 | $R^2$ = 0.973 AAPRE = 0.66% RSME = 2.338 |

**Table 4.** *Cont.*

| Reference | Data Source (Size) | Input Parameters | Target | Architecture and Optimization | Summary of Results |
|---|---|---|---|---|---|
| Kamari et al. (2019) [60] | Literature compilation [57–59,61–63]; 254 pts | Pressure, molar mass | WDT | MLP-LMA of shape 2-5-1 | $R^2$ = 0.950<br>AAPRE = 0.60%<br>RMSE = 2.200 |
| Mansourpoor et al. (2019) [89] | Literature compilation [57,58,62]; 310 pts | Molar mass, pressure, specific gravity | WDT | MLP-LMA of shape 3-16-1 | $R^2$ = 0.972<br>AAPRE = 0.38%<br>RMSE = 1.779 |
| Benamara et al. (2020) [90] | 59 Algerian oil samples (experimental) | Density, wax tenor, pour point, freezing point, wax content | WAT | MLP-LMA of shape 5-11-10-9-1 | $R^2$ = 0.859<br>AAPRE = 0.74%<br>RMSE = 2.350 |
| | | | | MLP-BR of shape 5-12-12-9-1 | $R^2$ = 0.907<br>AAPRE = 0.67%<br>RMSE = 2.221 |
| Amar et al. (2022) [91] | Literature compilation [50,54,55]; 88 pts | $C_1$–$C_3$, $C_4$–$C_7$, $C_8$–$C_{15}$, $C_{16}$–$C_{22}$, $C_{23}$–$C_{29}$, $C_{30+}$, specific gravity, temperature | Wax precipitation weight | MLP-LMA of shape 8-11-11-9-1 | $R^2$ = 0.994<br>RMSE = 0.359 |
| | | | | MLP-BR of shape 8-11-11-9-1 | $R^2$ = 0.991<br>RMSE = 0.518 |
| Askari et al. (2021) [92] | Own experimental data | Pipe size, dual-source gamma-ray detector counts | Wax deposition thickness | MLP-LMA of shape 2-18-1 | RMSE = 0.040 |
| Amiri-Ramsheh et al. (2022) [93] | Literature compilation [56–60,62,63,79,88]; 346 pts | Pressure, molar mass | WDT | MLP-LMA of shape 2-10-15-1 | AAPRE = 0.77%,<br>RMSE = 4.194 |
| | | | | MLP-BR of shape 2-10-10-1 | AAPRE = 0.87%,<br>RMSE = 4.998 |
| | | | | RBFNN of spread 0.1, max 65 neurons | AAPRE = 0.64%,<br>RMSE = 2.740 |
| Septiano et al. (2022) [64] | Literature compilation [52,65,66]; 75 points, augmented to 13,995 simulated | Water volume fraction, wall shear stress, dynamic viscosity, temperature gradient at pipeline wall, wax concentration gradient | Wax deposition rate | MLP-LMA of shape 6-56-56-1 | $R^2$ = 0.992<br>RMSE = 0.179 |
| Xiao et al. (2022) [94] | Huachi oilfield [87]; 38 pts | Temperature, wall temperature, viscosity, wall shear stress, flow velocity, temperature gradient at pipeline wall, wax concentration gradient | Wax deposition rate | MLP of shape 7-7-1 | $R^2$ = 0.944<br>AAPRE = 8.78%<br>RMSE = 0.894 |
| | | | | MLP-GA of shape 7-7-1 | $R^2$ = 0.991<br>AAPRE = 3.78%<br>RMSE = 0.397 |
| | | | | MLP-WOA of shape 7-7-1 | $R^2$ = 0.997<br>AAPRE = 2.72%<br>RMSE = 0.313 |
| Amiri-Ramsheh et al. (2023) [95] | Literature compilation [49,96–98]; 173 pts | American Petroleum Institute gravity (°API), pour point | Wax precipitation weight | MLP-LMA of shape 2-10-8-1 | $R^2$ = 0.944<br>AAPRE = 16.59%<br>RMSE = 1.370 |
| | | | | MLP-BR of shape 2-10-8-1 | $R^2$ = 0.876<br>AAPRE = 19.68%<br>RMSE = 2.038 |

**Table 4.** *Cont.*

| Reference | Data Source (Size) | Input Parameters | Target | Architecture and Optimization | Summary of Results |
|---|---|---|---|---|---|
| | | | | MLP-BFGS of shape 2-10-8-1 | $R^2$ = 0.959<br>AAPRE = 17.18%<br>RMSE = 1.142 |
| | | | | RBFNN with 90 hidden layer neurons, spread = 1.2 | $R^2$ = 0.866<br>AAPRE = 26.33%<br>RMSE = 2.031 |
| | | | | CFNN-LMA, with 10 nodes in first and 15 nodes in second hidden layer | $R^2$ = 0.785<br>AAPRE = 21.84%<br>RMSE = 2.959 |
| | | | | CFNN-SCG, with 10 nodes in first and 15 nodes in second hidden layer | $R^2$ = 0.845<br>AAPRE = 26.33%<br>RMSE = 1.907 |
| | | | | CFNN-BFGS, with 10 nodes in first and 15 nodes in second hidden layer | $R^2$ = 0.897<br>AAPRE = 21.11%<br>RMSE = 1.757 |
| | | | | GRNN with spread = 0.03 | $R^2$ = 0.960<br>AAPRE = 10.26%<br>RMSE = 1.113 |
| Sultana et al. (2023) [99] | Not reported; 106 pts | Wall shear stress, viscosity, wax concentration gradient, temperature gradient at pipeline wall | Wax deposition rate | RBFNN with structure of 4-84-1 goal of 0.001 and spread of 2 | $R^2$ = 0.991<br>AAPRE = 1.50%<br>RMSE = 0.860 |
| Aguilar-Hernández et al. (2025) [100] | Experimental data; 5 samples | Pressure, paraffin content, $C_1$–$C_7$, $C_8$–$C_{15}$, $C_{16}$–$C_{23}$, $C_{24}$–$C_{30}$ | WAT | Deep MLP, 3 hidden layers (284-1182-284), ReLU, Adam, L2, dropout, early stopping | $R^2$ = 0.998,<br>RMSE = 0.379<br>AAPRE = 9.00%, |
| Sarkodie et al. (2026) [73] | Literature compilation [66,74,75]; 215 pts | Temperature, wall temperature, viscosity, wall shear stress, flow velocity, temperature gradient at pipeline wall, wax concentration gradient | Wax deposition rate | MLP | $R^2$ = 0.950<br>AAPRE = 15.47%<br>RMSE = 0.185 |
| Youcefi et al. (2026) [101] | Literature compilation [102–104]; 101 pts | Critical temperature of wax, temperature, pressure, critical temperature of gas system | Wax solubility | MLP-LMA of shape 4-10-8-1 | $R^2$ = 0.996<br>RMSE = 92.904 |
| | | | | MLP-BR of shape 4-10-6-1 | $R^2$ = 0.994<br>RMSE = 114.381, |

**Table 5.** Summary of neuro-fuzzy models used for wax deposition prediction (unless noted, $R^2$, AAPRE and RMSE are test-set values).

| Reference | Data Source (Size) | Input Parameters | Target | Architecture and Optimization | Summary of Results |
|---|---|---|---|---|---|
| Jalalnezhad and Kamali (2016) [105] | Literature compilation [84–86,106]; 1500 pts | Reynolds number, residence time, temperature driving force, wax content | Wax deposition thickness | ANFIS with range of influence of 0.23, squash factor of 0.25, accept ratio of 0.5, reject ratio of 0.15 | $R^2$ = 0.986<br>AAPRE = 0.01%<br>RMSE = 0.028 |

**Table 5.** *Cont.*

| Reference | Data Source (Size) | Input Parameters | Target | Architecture and Optimization | Summary of Results |
|---|---|---|---|---|---|
| Chu et al. (2017) [107] | Literature compilation [50,54,82] | $C_1$–$C_3$, $C_4$–$C_7$, $C_8$–$C_{15}$, $C_{16}$–$C_{22}$, $C_{23}$–$C_{29}$, $C_{30+}$, specific gravity, pressure, temperature | Wax precipitation weight | ANFIS-PSO | $R^2$ = 0.994<br>AAPRE = 21.57%<br>RMSE = 0.290 |
| Saeedi Dehaghani et al. (2017) [83] | Literature compilation [84–86]; 1560 pts | Reynolds number, residence time, temperature driving force, wax content | Wax deposition thickness | ANFIS | $R^2$ = 0.986<br>AAPRE = 9.80% |
| Bian et al. (2019) [56] | Literature compilation [57–59]; 272 pts | Pressure, molar mass | WDT | ANFIS-GA | $R^2$ = 0.870<br>AAPRE = 1.27%<br>RMSE = 4.538 |
| | | | | ANFIS-PSO | $R^2$ = 0.923<br>AAPRE = 1.34%<br>RMSE = 5.268 |
| Amiri-Ramsheh et al. (2022) [93] | Literature compilation [56–60,62,63,79,88]; 346 pts | Pressure, molar mass | WDT | ANFIS-BBO (keep rate 0.2, α 0.9, 1000 iter, pop 100) | AAPRE = 0.69%,<br>RMSE = 3.095 |
| | | | | ANFIS-TLBO (1000 iter, pop 100) | AAPRE = 0.73%,<br>RMSE = 2.945 |
| | | | | ANFIS-CA (accept rate 0.2, influence type 3, α = 0.9, β = 1, 1000 iter, pop 400) | AAPRE = 0.87%,<br>RMSE = 4.672 |
| Ahmadi (2023) [108] | Lit. compilation [50,54,82]; 88 pts | $C_1$–$C_3$, $C_4$–$C_7$, $C_8$–$C_{15}$, $C_{16}$–$C_{22}$, $C_{23}$–$C_{29}$, $C_{30+}$, specific gravity, temperature | Wax precipitation weight | FIS | $R^2$ = 0.882<br>RMSE = 0.136 |
| | | | | FIS-GA with cross-over rate of 3, 22 genes, population of 18, 125 generations, and mutation rate of 0.0075 | $R^2$ = 0.945<br>RMSE = 0.056 |
| | | | | HFGA (Hybrid of ANN, FIS and GA) | $R^2$ = 0.968<br>RMSE = 0.048 |
| Kouhi et al. (2025) [68] | Literature compilation [69–71]; 81 pts | Density, wax content, pour point | WAT | ANFIS | $R^2$ = 0.966<br>RMSE = 2.712<br>AAPRE = 9.71% |

**Table 6.** Summary of tree-based models used for wax deposition prediction (unless noted, $R^2$, AAPRE and RMSE are test-set values).

| Reference | Data Source (Size) | Input Parameters | Target | Architecture and Optimization | Summary of Results |
|---|---|---|---|---|---|
| Kamari et al. (2019) [60] | Literature compilation [57–59,61–63]; 254 pts | Pressure, molar mass | WDT | DT | $R^2$ = 0.970<br>AAPRE = 0.30%<br>RMSE = 1.500 |
| Amiri-Ramsheh et al. (2022) [93] | Literature compilation [56–60,62,63,79,88]; 346 pts | Pressure, molar mass | WDT | RF (min leaf 1, min parent 4, 250 estimators) | AAPRE = 0.29%<br>RMSE = 1.265 |
| | | | | DT (min leaf 1, min parent 4.97, max split 1) | AAPRE = 0.58%<br>RMSE = 2.570 |

**Table 6.** *Cont.*

| Reference | Data Source (Size) | Input Parameters | Target | Architecture and Optimization | Summary of Results |
|---|---|---|---|---|---|
| | | | | ET (min leaf 1, min parent 3, 10 estimators) | AAPRE = 0.53% RMSE = 2.143 |
| Septiano et al. (2022) [64] | Literature compilation [52,65,66]; 75 points, augmented to 13,995 simulated | Water volume fraction, wall shear stress, dynamic viscosity, temperature gradient at pipeline wall, wax concentration gradient | Wax deposition rate | RF (500 estimators) | $R^2$ = 0.993 RMSE = 0.178 |
| Ahmadi (2025) [109] | Literature compilation [50,54,55]; 88 pts | $C_1$–$C_3$, $C_4$–$C_7$, $C_8$–$C_{15}$, $C_{16}$–$C_{22}$, $C_{23}$–$C_{29}$, $C_{30+}$, specific gravity, temperature | Wax precipitation weight | XGBoost (100 trees, depth 3, learning rate: 0.1) | $R^2$ = 0.813 RMSE = 0.339 |
| | | | | RF (300 trees, min samples leaf:1, min samples split:2, max depth:12) | $R^2$ = 0.738 RMSE = 0.401 |
| Rifat et al. (2026) [110] | Literature compilation [57–59,68,98,111]; 98 pts | Wax content, density, pour point | WAT | XGBoost (250 trees, learning rate: 0.05) | $R^2$ = 0.958 AAPRE = 0.71% RMSE = 2.383 |
| | | | | Gradient Boosting (100 trees, learning rate: 0.05, max depth: 4) | $R^2$ = 0.953 AAPRE = 0.67% RMSE = 2.520 |
| | | | | XGBoost-Gradient-Boosting Stacking Ensemble | $R^2$ = 0.962 AAPRE = 0.67% RMSE = 2.273 |
| | | | | CatBoost (1000 iterations, learning rate: 0.01, depth: 4) | $R^2$ = 0.973 AAPRE = 0.55% RMSE = 1.935 |
| | | | | CatBoost-GWO (800 iterations, learning rate: 0.0214, depth: 4) | $R^2$ = 0.974 AAPRE = 0.55% RMSE = 1.882 |
| | | | | CatBoost-WOA (821 iterations, learning rate: 0.0119, depth: 4) | $R^2$ = 0.973 AAPRE = 0.56% RMSE = 1.918 |
| | | | | CatBoost-PSO (803 iterations, learning rate: 0.0315, depth: 4) | $R^2$ = 0.976 AAPRE = 0.51% RMSE = 1.811 |
| Sarkodie et al. (2026) [73] | Literature compilation [66,74,75]; 215 pts | Temperature, wall temperature, viscosity, wall shear stress, flow velocity, temperature gradient at pipeline wall, wax concentration gradient | Wax deposition rate | RF | $R^2$ = 0.998 AAPRE = 1.90% RMSE = 0.033 |
| | | | | Gradient Boosting | $R^2$ = 0.985 AAPRE = 5.09% RMSE = 0.101 |
| Yadav et al. (2026) [112] | Literature compilation [90,98,111]; 80 pts | Density, pour point, wax content | WAT | XGBoost (25 trees, max depth: 6, learning rate: 0.68) | $R^2$ = 0.972 AAPRE = 0.69% RMSE = 2.370. |
| | | | | Decision Tree (max depth: 5, min split: 2, min leaf: 2) | $R^2$ = 0.947 AAPRE = 0.87% RMSE = 3.360 |

**Table 6.** *Cont.*

| Reference | Data Source (Size) | Input Parameters | Target | Architecture and Optimization | Summary of Results |
|---|---|---|---|---|---|
| | | | | RF (15 trees, max depth: 4, min split: 2, min leaf: 1) | $R^2$ = 0.961 AAPRE = 0.88%, RMSE = 3.608 |
| | | | | ET (8 trees, max depth: 6, min split: 2, min leaf: 1) | $R^2$ = 0.951 AAPRE = 0.77%, RMSE = 3.038 |
| Gao et al. (2026) [72] | 85 field samples, Qinghai oilfield pipeline, then augmented to 1060 via WGAN-GP | Temperature, flow velocity, wax content, pressure, viscosity | Wax deposition rate | Two-layer stacking ensemble (RF + XGBoost + SVR base; Ridge meta) + WGAN-GP augmentation | $R^2$ = 0.963 RMSE = 0.527 |
| | | | | RF only (200 trees, min leaf: 5, max split: 100) | $R^2$ = 0.937 RMSE = 0.689 |
| | | | | XGBoost only (200 trees, learning rate: 0.1) | $R^2$ = 0.952 RMSE = 0.603, |
| Youcefi et al. (2026) [101] | Literature compilation [102–104]; 101 pts | Critical temperature of wax, temperature, pressure, critical temperature of gas system | Wax solubility | Extra-Trees (573 trees, max depth: 10, min samples split: 3, min leaf: 1) | $R^2$ = 0.980 RMSE = 94.266 |

**Table 7.** Summary of other AI-based models used for wax deposition prediction (unless noted, $R^2$, AAPRE, and RMSE are test-set values).

| Reference | Data Source (Size) | Input Parameters | Target | Architecture and Optimization | Summary of Results |
|---|---|---|---|---|---|
| Manshad et al. (2012) [55] | Pedersen et al. (1991) [50]; 87 pts | $C_1$–$C_3$, $C_4$–$C_7$, $C_8$–$C_{15}$, $C_{16}$–$C_{22}$, $C_{23}$–$C_{29}$, $C_{30+}$, specific gravity, pressure, temperature | Wax precipitation weight | GPNN | $R^2$ = 0.931 |
| Gholami et al. (2018) [53] | Literature compilation [50,54,55] | $C_1$–$C_3$, $C_4$–$C_7$, $C_8$–$C_{15}$, $C_{16}$–$C_{22}$, $C_{23}$–$C_{29}$, $C_{30+}$, specific gravity, temperature | Wax precipitation weight | CM-GA. | $R^2$ = 0.975 MSE = 0.250 RMSE = 0.500 |
| Benamara et al. (2019) [88] | Lit. compilation [57–59]; 272 pts | Pressure, molar mass | WDT | GMDH of one input, one middle and one output layer | $R^2$ = 0.976 AAPRE = 0.69% RMSE = 2.337 |
| Benamara et al. (2020) [90] | 59 Algerian oil samples (experimental) | Density, wax tenor, pour point, freezing point, wax content | WAT | GEP of 150 chromosomes, 11 gene, population of 420, mutation rate of 0.45, inversion rate of 0.12 | $R^2$ = 0.720 AAPRE = 1.20% RMSE = 4.398 |
| Kim et al. (2022) [113] | OLGA simulator: 176,000 pts (2200 datasets) + 48 fine-tuning pts | Mass flow rate, inlet temperature, inlet pressure, outlet temperature, outlet pressure | Wax deposited volume, pressure, temperature of the pipeline grid | SAE, with 80 inputs and output neurons for the first training, and 5 inputs and 80 output neurons for the second training. | $R^2$ = 0.760 (Wax volume %) $R^2$ = 0.960 (Pressure) $R^2$ = 0.880 (Temperature) $R^2$ = 0.900 (Maximum wax volume %) |

**Table 7.** *Cont.*

| Reference | Data Source (Size) | Input Parameters | Target | Architecture and Optimization | Summary of Results |
|---|---|---|---|---|---|
| Chen et al. (2024) [114] | Yang 2015, Wang 2010 [115,116]; 73 pts | Flow velocity, temperature, wall temperature, wall shear stress, viscosity, wax solubility, temperature gradient at pipeline wall | Wax deposition rate | WOA-ENN | $R^2$ = 0.999 AAPRE = 0.80% RMSE = 0.182 (Averaged performance of 2 datasets) |
| | | | | RSA-ENN | $R^2$ = 0.999 AAPRE = 0.54% RMSE = 0.116 (Averaged performance of 2 datasets) |
| | | | | IRSA-ENN | $R^2$ = 0.999 AAPRE = 0.33% RMSE = 0.070 (Averaged performance of 2 datasets) |
| Amar et al. (2024) [117] | Literature compilation [57–59]; 272 pts | Pressure, molar mass | WDT | GEP | $R^2$ = 0.968 AAPRE = 0.55% RMSE = 2.063 |
| Jin et al. (2025) [118] | Literature compilation [115,119,120]; 105 pts | Flow velocity, temperature, wall temperature, wall shear stress, viscosity, wax solubility, temperature gradient at pipeline wall | Wax deposition rate | ENN | AAPRE = 13.22% RMSE = 5.392 (Averaged performance of 3 datasets) |
| | | | | AOA-ENN | AAPRE = 2.14% RMSE = 0.707 (Averaged performance of 3 datasets) |
| | | | | PSO-ENN | AAPRE = 3.31% RMSE = 1.121 (Averaged performance of 3 datasets) |
| | | | | GA-ENN | AAPRE = 4.43%, RMSE = 1.237 (Averaged performance of 3 datasets) |
| Ahmadi (2025) [109] | Literature compilation [50,54,55]; 88 pts | $C_1$–$C_3$, $C_4$–$C_7$, $C_8$–$C_{15}$, $C_{16}$–$C_{22}$, $C_{23}$–$C_{29}$, $C_{30+}$, specific gravity, temperature | Wax precipitation weight | PINN | $R^2$ = 0.807 RMSE = 0.344 |
| Sarkodie et al. (2026) [73] | Literature compilation [66,74,75]; 215 pts | Temperature, wall temperature, viscosity, wall shear stress, flow velocity, temperature gradient at pipeline wall, wax concentration gradient | Wax deposition rate | KNN | $R^2$ = 0.985 AAPRE = 8.16% RMSE = 0.101 |

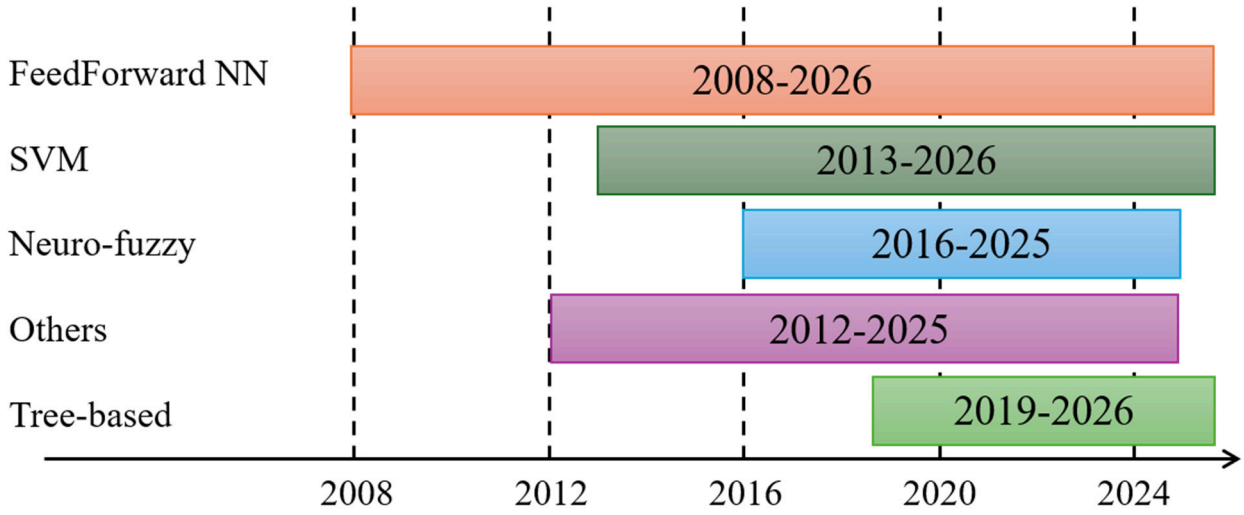


**Figure 5.** Adoption timeline of AI model families used for wax deposition prediction (2008–2026).

### *4.1. SVM-Based Models*

In 2013, Kamari et al. [49] trained an LSSVM on Pedersen et al.'s 87-point dataset [50], reaching $R^2$ = 0.989 and RMSE = 0.440 (AAPRE = 36.30%). In 2014, Kamari et al. [51] applied an LSSVM tuned by coupled simulated annealing to the wax deposition rate, based on Wei et al.'s 10-point dataset [52], reporting $R^2$ = 0.999, RMSE = 0.006, and AAPRE = 0.05%. In 2018, Gholami et al. [53] compared SVR with sigmoid, RBF, and linear kernels for the wax deposition rate from several studies [50,54,55]. The RBF kernel was the best ($R^2$ = 0.968, RMSE ≈ 0.570), with the others reaching only $R^2$ ≈ 0.83. In 2019, Bian et al. [56] built SVM-GWO and LSSVM models for WDT from 272 points [57–59]. Both led their comparison with $R^2$ > 0.94, AAPRE < 1%, and RMSE < 3. The same year, Kamari et al. [60] predicted WDT with an LSSVM on 254 points [57–59,61–63] ($R^2$ = 0.95, AAPRE = 0.60%, RMSE = 2.20). In 2022, Septiano et al. [64] built an SVR model for the wax deposition rate, trained on 13,995 points simulated from 75 experimental measurements and reached $R^2$ = 0.945 and RMSE = 0.493. In 2024, Khalighi and Cheremisin [67] optimized an LSSVM with a GA on 88 samples [50]. By removing two low-relevance inputs ($C_1$–$C_3$ mole fraction and specific gravity), it raised the model from $R^2$ = 0.939 to $R^2$ = 0.988 (RMSE = 0.360). In 2025, Kouhi et al. [68] predicted WAT from 81 points using oil density, wax content, and pour point. When benchmarked against an RNN and ANFIS, the LSSVM was the most accurate ($R^2$ = 0.999, RMSE = 0.007, AARD = 3.41%), with pour point being the dominant input. In 2026, Sarkodie et al. [73] generated an SVR for the wax deposition rate on 215 compiled points under 5-fold cross-validation, resulting in $R^2$ = 0.970, AAPRE = 12.32%, and RMSE = 0.144. In the same year, Gao et al. [72] reported a standalone SVR ($R^2$ = 0.961) as the strongest single base learner in their stacking ensemble.

### *4.2. Feedforward Neural Network Models*

MLP is by far the most common architecture. In 2008, Huang and Ma [76] trained a 4-4-1 MLP on 26 Daqing oilfield points for the wax deposition rate, reporting a correlation coefficient of 0.95 against field data. In the same year, Obanijesu and Omidiora [77] used an MLP to predict and classify wax deposition potential across 11 Nigerian reservoirs (Pearson r = 0.97). In 2010, Wei et al. [52] predicted a wax deposition rate with a 4-7-1 MLP (AAPRE < 2%). In 2012, Manshad et al. [55] predicted the wax deposition amount with an MLP on 87 points [50] ($R^2$ = 0.983), with $C_8$–$C_{15}$, $C_{16}$–$C_{22}$, and temperature being the most influential. In 2013, Kelechukwu et al. [78] trained a 3-12-1 MLP-LMA on 360 Malaysian crude points ($R^2$ = 0.983). In the same year, Moradi et al. [79] compared LMA, SCG, GDA,

and BR training of a 2-16-1 MLP for WDT on 306 points [57–59,61–63]; LMA was best ($R^2$ = 0.988, AAPRE = 0.49%) and beat thermodynamic models under varying pressure. In 2015, Behbahani et al. [80] used a 3-4-10-1 MLP-LMA for wax precipitation and WAT on Iranian crude (AAPRE < 4%), exceeding solid-solution and multi-solid models. In 2017, Eghtedaei et al. [81] applied an RBFNN-LMA network to predict wax deposition amount, reaching $R^2$ = 0.998, AAPRE = 11.74%, and RMSE = 0.171. In the same year, Saeedi Dehaghani et al. [83] modeled a 4-19-8-1 MLP-LMA for predicting wax deposition thickness on 1560 points, resulting in $R^2$ = 0.999 and AAPRE = 4.54%. In 2018, Gholami et al. [53] reached $R^2$ = 0.972 (RMSE ≈ 0.548) with an MLP-LMA, slightly better than their SVR. In 2019, Kamari et al. [60] reported an MLP-LMA for WDT ($R^2$ = 0.95, AAPRE = 0.60%, RMSE = 2.20). In the same year, Mansourpoor et al. [89] used a 3-16-1 MLP-LMA for WDT on 310 points, reporting $R^2$ = 0.972, AAPRE = 0.38%, and RMSE = 1.78. In 2020, Benamara et al. [90] predicted WAT from 59 Algerian samples with a 5-11-10-9-1 MLP-LMA and a 5-12-12-9-1 MLP-BR; MLP-BR was better ($R^2$ = 0.907, AAPRE = 0.67%, RMSE = 2.221), with freezing and pour points being the most influential. In 2021, Askari et al. [92] coupled gamma-ray densitometry with an MLP-LMA to infer wax deposition thickness directly from backscattered photon counts (RMSE < 0.05), a sensor-based approach distinct from the thermophysical-input models. In 2022, Amar et al. [91] trained 8-11-11-9-1 MLP-LMA and MLP-BR on 88 points [50,54,55], both at $R^2$ ≈ 0.99 (RMSE ≈ 0.3–0.5). In the same year, Xiao et al. [94] optimized a 7-7-1 MLP for the wax deposition rate on 38 points; MLP-WOA ($R^2$ = 0.997, AAPRE = 2.72%, RMSE = 0.313) outperformed MLP-GA ($R^2$ = 0.991, AAPRE = 3.78%, RMSE = 0.397) and the un-optimized network ($R^2$ = 0.944, AAPRE = 8.78%, RMSE = 0.894). In the same year, Septiano et al. [64] also compared their MLP-LMA model with $R^2$ = 0.992 and RMSE = 0.179. In 2023, Amiri-Ramsheh et al. [95] compared feedforward models on 173 wax content measurements [49,96–98]; the 2-10-8-1 MLP-BFGS was best ($R^2$ = 0.959, RMSE = 1.142, AAPRE = 17.18%), ahead of MLP-LMA. In 2025, Aguilar-Hernández et al. [100] trained a three-hidden-layer MLP (284-1182-284, Adam) to estimate WAT from pressure, paraffin content, and lumped fractions, reaching $R^2$ = 0.998 (RMSE = 0.379, AAPRE = 9.00%), beating a single-hidden-layer MLP ($R^2$ = 0.961) and linear regression ($R^2$ = 0.920), with pressure being the most dominant predictor feature. In 2026, Sarkodie et al. [73] also compared with an MLP with performance of $R^2$ = 0.950, AAPRE = 15.47%, and RMSE = 0.185. In the same year, Youcefi et al. [101] collected 101 data points [102–104] to predict wax solubility in $CO_2$ and $C_2H_6$, with 2 MLPs and extra-trees. MLP-BR ($R^2$ = 0.994, RMSE = 114.381) and MLP- LM ($R^2$ = 0.996, RMSE = 92.904) perform best, ahead of the extra-trees model.

Other feedforward variants appear less often. In 2017, Xie and Xing [66] reached AAPRE < 1.5% with an RBFNN on 38 points [87]. In 2019, Benamara et al. [88] compared GA- and ABC-tuned RBFNNs for WDT on 272 points [57–59], with the ABC variant being slightly better. In 2022, Amiri-Ramsheh et al. [93] compiled 346 WDT points from multiple literature sources [57–59,62,63,79] and benchmarked feedforward, neuro-fuzzy, and tree-based families using only pressure and molar mass as inputs. Among the feedforward variants, the RBFNN (AAPRE = 0.635%, RMSE = 2.740) outperformed both MLP-LMA (AAPRE = 0.765%, RMSE = 4.194) and MLP-BR (AAPRE = 0.869%, RMSE = 4.998). In 2023, Sultana et al. [99] reported $R^2$ = 0.991, AAPRE = 1.50%, and RMSE = 0.860, with an RBFNN on 106 points. In the same year, Amiri-Ramsheh et al. [95] also tested RBFNN ($R^2$ = 0.866), CFNN (CFNN-BFGS best) ($R^2$ = 0.785–0.897), and GRNN ($R^2$ = 0.960), all trailing their MLPs.

### 4.3. Neuro-Fuzzy Models

In 2016, Jalalnezhad and Kamali [105] built an ANFIS for wax deposition thickness in turbulent flow from 1500 points [84–86,106] using Reynolds number, time, a dimensionless temperature driving force, and wax content ($R^2$ = 0.986, RMSE = 0.028, AAPRE = 0.10%). In 2017, Chu et al. [107] tuned an ANFIS with PSO on the literature data [50,54,82] ($R^2$ = 0.994, AAPRE = 21.57%, RMSE ≈ 0.290). In the same year, Saeedi Dehaghani et al. [83] also compared an ANFIS model, resulting in $R^2$ = 0.986 and AAPRE = 9.80%, which was outperformed by the MLP counterpart. In 2019, Bian et al. [56] found ANFIS-GA and ANFIS-PSO trailed their SVM models for WDT ($R^2$ ≈ 0.87–0.92, AAPRE = 1.2–1.3%, RMSE = 4.5–5.2). In 2022, Amiri-Ramsheh et al. [93] also tested three metaheuristic-tuned ANFIS variants: ANFIS-TLBO (AAPRE = 0.727%, RMSE = 2.945), ANFIS-BBO (AAPRE = 0.694%, RMSE = 3.095), and ANFIS-CA (AAPRE = 0.870%, RMSE = 4.672). However, these three models all trailed the tree-based models in the same study. In 2023, Ahmadi [108] proposed HFGA, a hybrid of MLP, fuzzy logic, and GA with eight inputs, which beat standalone FIS and FIS-GA on 88 points [50,54,82] ($R^2$ = 0.968, RMSE ≈ 0.048). In 2025, Kouhi et al. [68] found the ANFIS variant to be the weakest of the three architectures for WAT ($R^2$ = 0.966, RMSE = 2.712, AAPRE = 9.71%).

### 4.4. Tree-Based Models

Tree-based models are the most recent entrants and currently the strongest on small tabular wax data. In 2019, Kamari et al. [60] included a decision tree in their WDT comparison, where it outperformed their MLP-LMA and LSSVM ($R^2$ = 0.97, AAPRE = 0.30%, RMSE = 1.5). In 2022, Amiri-Ramsheh et al. [93] also compared decision trees, extra-trees, and random forests for WDT. The random forest was the best model overall (AAPRE = 0.288%, RMSE = 1.265), ahead of the decision tree (AAPRE = 0.579%, RMSE = 2.570) and extra-trees (AAPRE = 0.534%, RMSE = 2.143). Tree-based models outperformed every feedforward and neuro-fuzzy model in the same study. In the same year, Septiano et al.'s [64] random forest model achieved $R^2$ = 0.993 and RMSE = 0.178 performance, the best of their MLP-LMA, SVR, and RF models. In 2025, Ahmadi [109] compared XGBoost, random forest, and PINN on 88 samples [50,54,55] for wax deposition percentage. XGBoost ($R^2$ = 0.813, RMSE = 0.339) and random forest ($R^2$ = 0.738, RMSE = 0.401) performed better than PINN, with system temperature and the $C_8$–$C_{15}$/$C_{16}$–$C_{22}$ fractions dominant by SHAP analysis. In 2026, Rifat et al. [110] benchmarked gradient-boosting variants for WAT on 98 points, with CatBoost-PSO performing best ($R^2$ = 0.976, AAPRE = 0.51%, RMSE = 1.81). In the same year, Sarkodie et al. [73] also compared with a random forest and gradient boosting, where random forest was the best amongst all comparisons, with performance of $R^2$ = 0.998, AAPRE = 1.90%, and RMSE = 0.033. In the same year, Yadav et al. [112] compared random forest, decision trees, extra-trees, and XGBoost for WAT on 80 points [90,98,111]. XGBoost led ($R^2$ = 0.972, AAPRE = 0.69%, RMSE = 2.370), ahead of random forest ($R^2$ = 0.961, AAPRE = 0.88%, RMSE = 3.608), extra-trees ($R^2$ = 0.951, AAPRE = 0.77%, RMSE = 3.038), and decision trees ($R^2$ = 0.947, AAPRE = 0.87%, RMSE = 3.360). In the same year, Gao et al. [72] stacked random forest, XGBoost, and SVR base learners under a ridge meta-learner, trained on 1060 WGAN-GP-augmented samples from 85 Qinghai oilfield points, with XGBoost ($R^2$ = 0.952, RMSE = 0.603) as the best base learner and random forest ($R^2$ = 0.937, RMSE = 0.689) as the weakest base learner. In the same year, Youcefi et al. [101] found out that the extra-trees model ($R^2$ = 0.980, RMSE = 94.266) performs worst, behind the two MLP models.

### 4.5. Other Models

Several architectures appear only occasionally. In 2012, Manshad et al. [55] also tested a GPNN against their MLP ($R^2$ = 0.931). In 2018, Gholami et al. [53] combined SVR and

MLP-LMA in a GA-weighted committee machine, their best model overall ($R^2$ = 0.975, RMSE ≈ 0.5). In 2019, Benamara et al. [88] built a GMDH that beat their RBFNN ($R^2$ = 0.976, AAPRE = 0.69%, RMSE = 2.337). In 2020, Benamara et al. [90] also reported a GEP model, which was comparatively weak ($R^2$ = 0.720, AAPRE = 1.20%, RMSE = 4.398). In 2022, Kim et al. [113] trained a stacked auto-encoder on 176,000 OLGA-simulated points (fine-tuned on 48 experimental points), reaching $R^2$ = 0.76 for wax %, 0.88 for temperature, 0.96 for pressure, and 0.90 for maximum wax volume. In 2024, Chen et al. [114] optimized an Elman NN with IRSA (against WOA and RSA) on 35 and 38 data groups [115,116]. All three models achieved $R^2$ of 0.999, with IRSA-ENN being the most accurate (RMSE = 0.070, AAPRE = 0.33%). In the same year, Amar et al. [117] developed a white-box GEP correlation for WDT on 272 points, reporting $R^2$ = 0.968, AAPRE = 0.55%, and RMSE = 2.06. In 2025, Jin et al. [118] applied AOA to an Elman NN across three datasets (total of 105 sets of data) [115,119,120], cutting AAPRE from ~9–19% to 1.5–2.5% and beating PSO- and GA-tuned versions. In the same year, Ahmadi [109] showed that the PINN performs similarly ($R^2$ = 0.807, RMSE = 0.344) to the tree-based models. In 2026, Sarkodie et al. [73] also trained a KNN, resulting in $R^2$ = 0.985, AAPRE = 8.16%, and RMSE = 0.101.

## 5. Discussion

### *5.1. Performance Landscape Across Model Families*

Figure 6 shows the number of models reported in each family, disaggregated by the four principal prediction targets (WAT, WDT, wax-deposited-%/mass, and wax deposition rate). The distributions of the three reported metrics are shown in Figures 7–9, and the corresponding per-target summary statistics are collected in Table 8. Reported $R^2$ is heavily concentrated above 0.95 across all families (Figure 7). However, AAPRE (Figure 8) varies widely between targets, and RMSE (Figure 9) is scale-dependent, so it is shown per target rather than pooled.

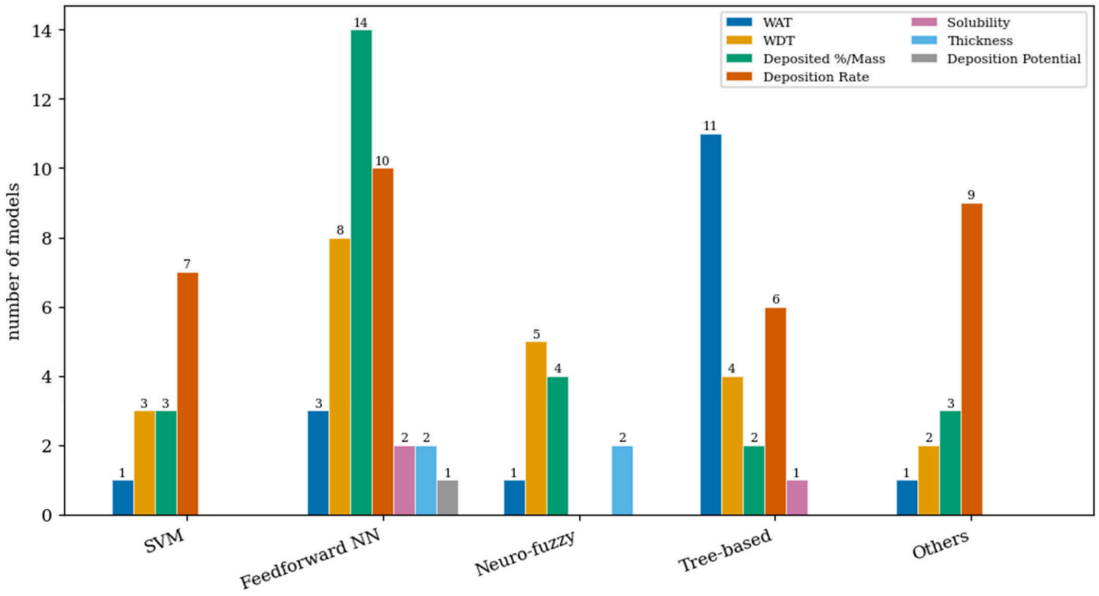


**Figure 6.** Number of reviewed AI-based models per model family, split by prediction target (WAT, WDT, wax deposited %/mass, wax deposition rate, wax solubility, wax thickness, and wax deposition potential).

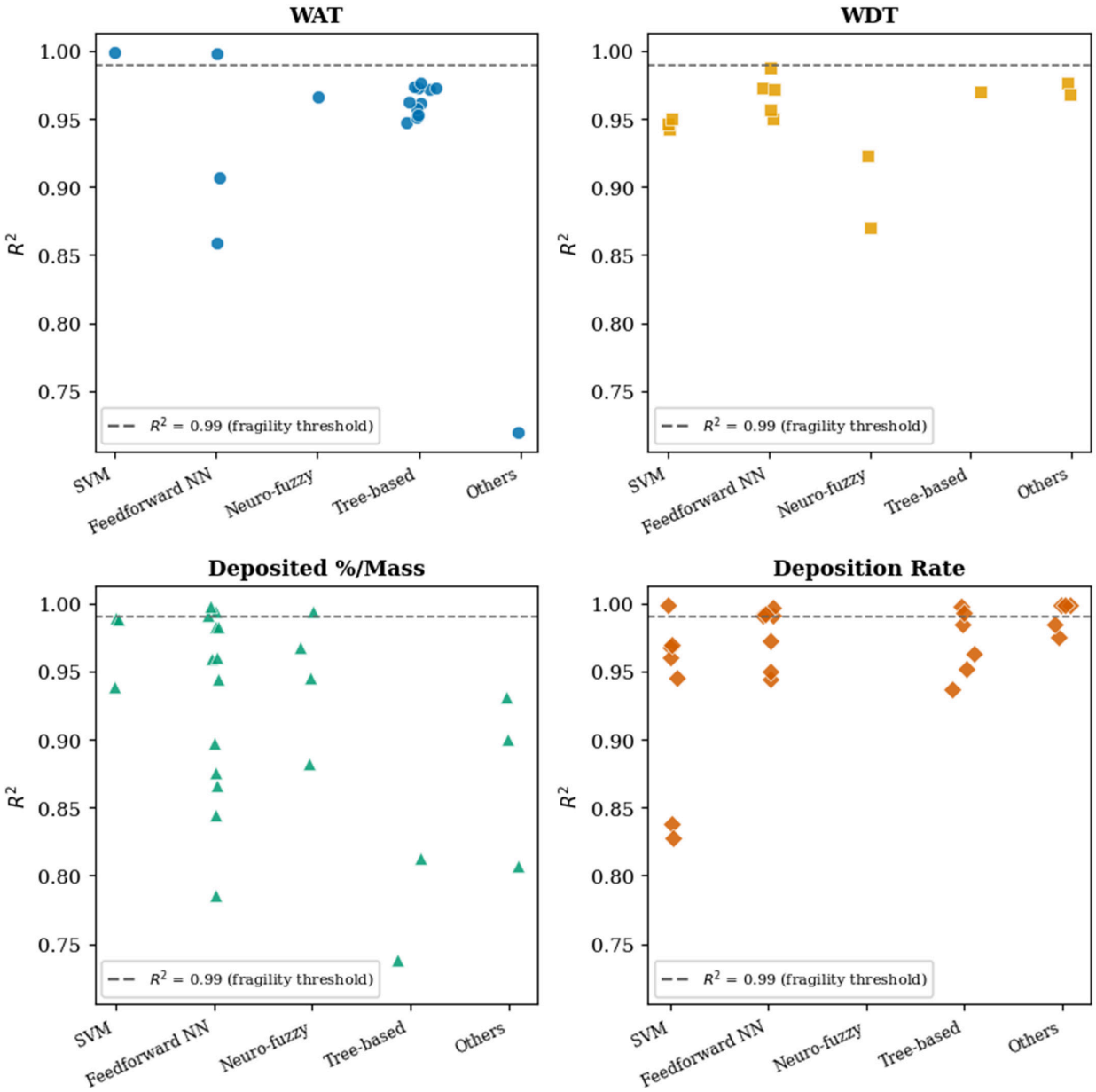


**Figure 7.** Distribution of recorded $R^2$ values by model family labeled by prediction target.

**Table 8.** Per-target summary statistics of reported model performance: number of studies and models, median and interquartile range of $R^2$ and AAPRE, bootstrap 95% confidence interval of the median $R^2$, and median dataset size.

| Target | Studies | Models | $R^2$ Median | $R^2$ IQR | $R^2$ 95% CI | AAPRE Median (%) | AAPRE IQR | Median n |
|---|---|---|---|---|---|---|---|---|
| WAT | 5 | 17 | 0.962 | [0.951, 0.973] | [0.951, 0.973] | 0.708 | [0.668, 0.880] | 80 |
| WDT | 7 | 22 | 0.957 | [0.946, 0.972] | [0.946, 0.972] | 0.647 | [0.555, 0.756] | 272 |
| Wax Deposited % or Mass | 12 | 26 | 0.944 | [0.876, 0.983] | [0.882, 0.983] | 20.395 | [15.377, 22.962] | 88 |
| Wax Deposition Rate | 12 | 32 | 0.975 | [0.952, 0.993] | [0.960, 0.992] | 2.72 | [1.500, 6.625] | 56 |
| Wax Solubility | 1 | 3 | 0.994 | [0.987, 0.995] | [0.980, 0.996] | | | |
| Wax Thickness | 3 | 4 | 0.986 | [0.986, 0.992] | [0.986, 0.999] | 4.537 | [2.278, 7.166] | 1530 |
| Wax Deposition Potential | 1 | 1 | 0.97 | [0.970, 0.970] | | | | |

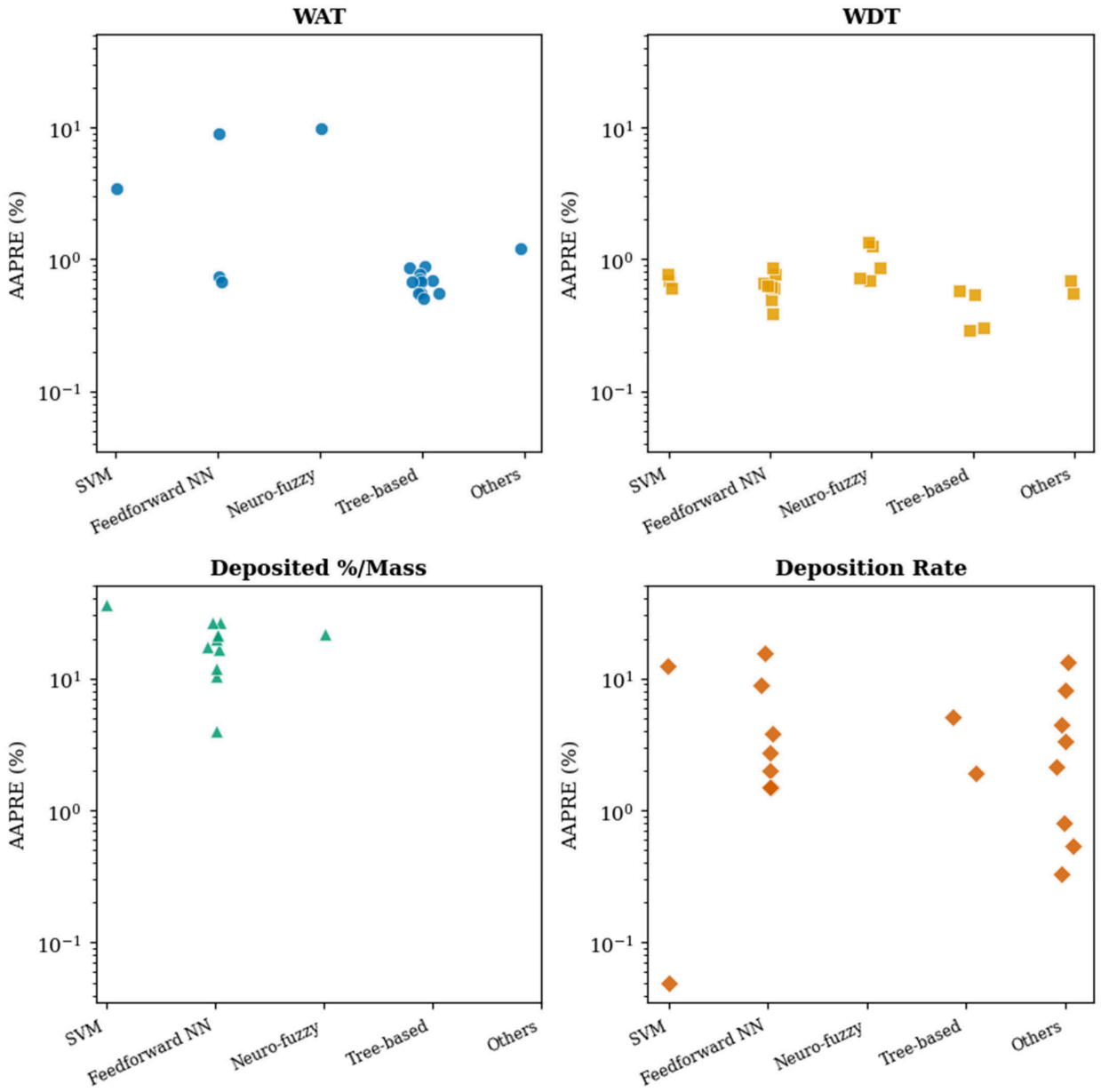


**Figure 8.** Distribution of recorded AAPRE% values by model family labeled by prediction target.

Feedforward neural networks, and the MLP in particular, dominate the literature by volume and report consistently high accuracy, with $R^2$ frequently above 0.95 (Figure 6). For the MLP, Levenberg–Marquardt (LMA) remains the default trainer, usually benchmarked against Bayesian regularization (BR). However, no consistent winner emerges: some studies favor LMA, others BR, and Amiri-Ramsheh et al. [95] report BFGS outperforming both. This inconsistency indicates that optimizer effectiveness is dataset-dependent rather than intrinsic, so optimizer choice should be treated as a tunable hyperparameter rather than settled by convention. Among SVM models, SVR with an RBF kernel is the most accurate kernel choice [66], while LSSVM is more prevalent and routinely exceeds $R^2 = 0.94$. Neuro-fuzzy models (ANFIS) reach comparable $R^2$ but trail SVMs in direct comparison [56].

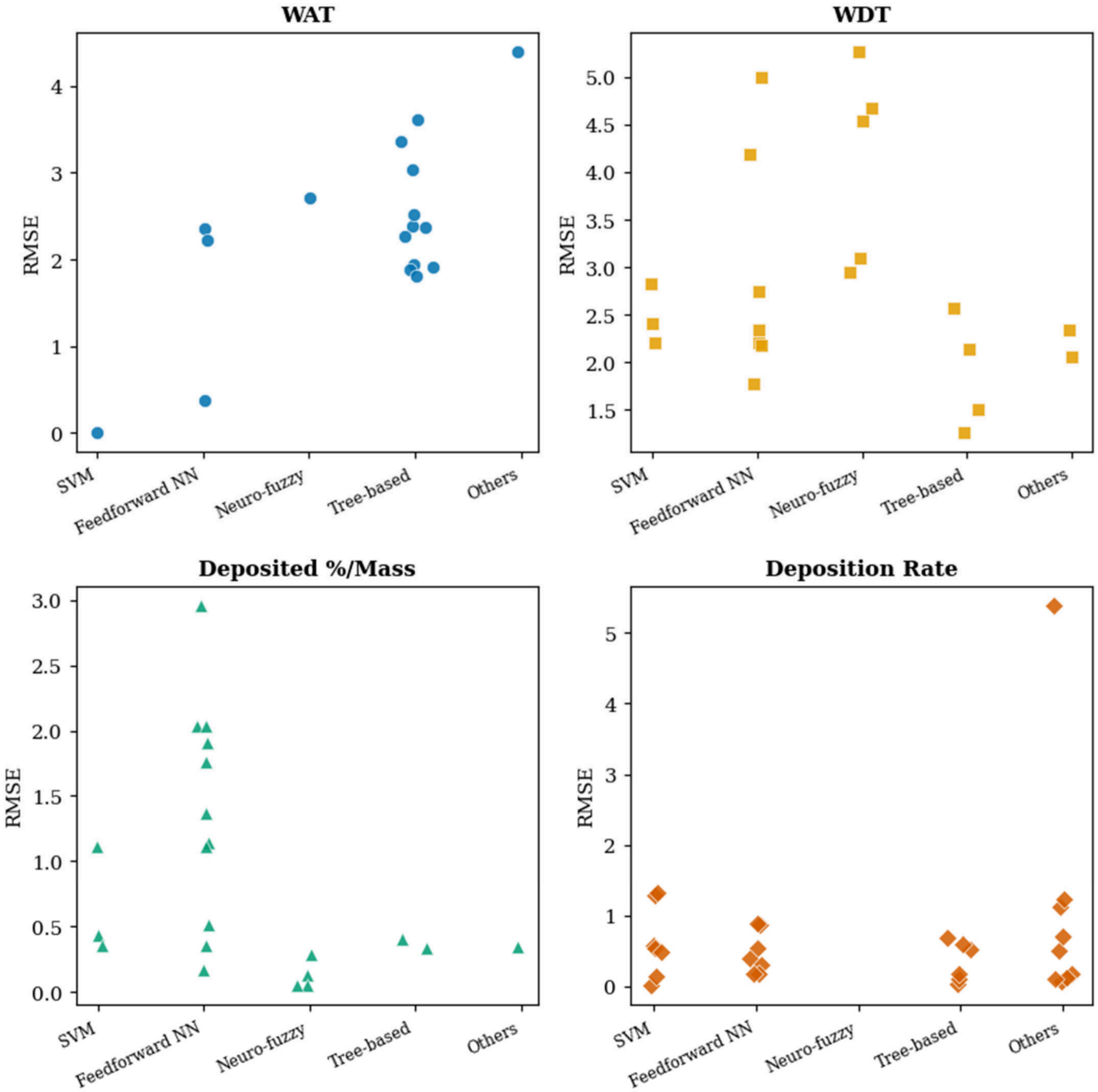


**Figure 9.** Distribution of recorded RMSE values by model family labeled by prediction target.

The clearest recent shift is the rise in tree-based models, most of which appeared in 2025–2026. In within-study comparisons, where models are trained and tested on identical data, gradient boosting is the most frequent winner, leading in 5 of the 13 multi-family studies and outperforming SVMs in every such comparison. However, no pairwise comparison reaches statistical significance, given the small number of head-to-head studies. The advantage is also target-dependent. For example, on the wax-weight datasets, gradient boosting is in fact the weakest family (Figure 7); XGBoost and random forest score below older feedforward networks on the same data [72,109,112]. Across studies, the median $R^2$ of tree-based models is no higher than that of established MLP or SVM work. Their real advantage is robustness on small tabular data and native interpretability through SHAP.

### *5.2. Dataset Scarcity and the Echo Chamber*

Figure 10 plots the reported $R^2$ against dataset size for every reviewed model, categorized by prediction target. Of the 87 models reporting an $R^2$, 36 achieve $R^2 > 0.95$ on fewer than 300 data points, and the median dataset across all studies is only 98 points

per study once simulated, and augmented sets are excluded (mean of 244 points). Nine models attain $R^2 > 0.99$ on fewer than 100 samples (Table 9); for example, $R^2 \approx 0.999$ [68] and $R^2 \approx 0.999$ [114] on 70–90 points. Such near-perfect scores on so few samples are statistically fragile and more likely reflect in-sample fitting than genuine generalization.

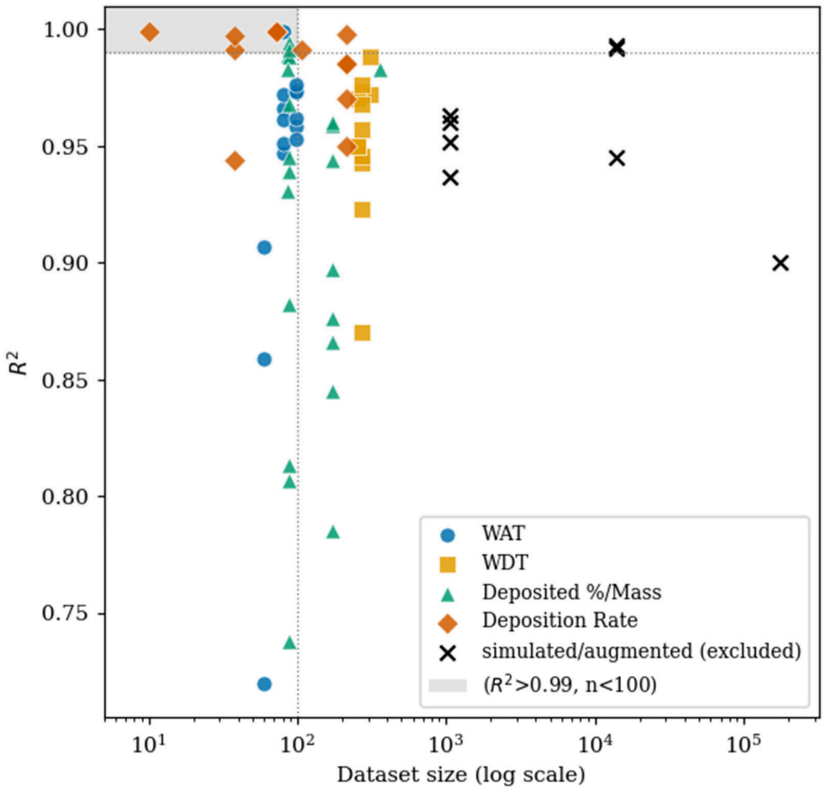


**Figure 10.** Reported $R^2$ versus dataset size for the reviewed AI-based wax-prediction models, grouped by prediction target. The gray band marks the zone with $R^2 > 0.99$ on fewer than 100 samples; the horizontal axis is logarithmic.

**Table 9.** Models reporting $R^2 > 0.99$ on fewer than 100 data points with their source datasets.

| Reference | Target | $R^2$ | n | Dataset (Source) |
|---|---|---|---|---|
| Kamari et al., 2014 (LSSVM) [51] | Wax Deposition Rate | 0.999 | 10 | Wei 2010 [52] |
| Xiao et al., 2022 (MLP-GA) [94] | Wax Deposition Rate | 0.991 | 38 | Wang 2010 [87] |
| Xiao et al., 2022 (MLP-WOA) [94] | Wax Deposition Rate | 0.997 | 38 | Wang 2010 [87] |
| Chen et al., 2024 (ENN-IRSA) [114] | Wax Deposition Rate | 0.999 | 73 | Wang 2010 [87] |
| Chen et al., 2024 (ENN-WOA) [114] | Wax Deposition Rate | 0.999 | 73 | Wang 2010 [87] |
| Chen et al., 2024 (ENN-RSA) [114] | Wax Deposition Rate | 0.999 | 73 | Wang 2010 [87] |
| Kouhi et al., 2025 (LSSVM) [68] | WAT | 0.999 | 81 | own WAT (81) |
| Amar et al., 2022 (MLP-BR) [91] | Wax Deposited % or Mass | 0.991 | 88 | Baltzer et al., Pedersen et al. compilation [50,54,55] |
| Amar et al., 2022 (MLP-LM) [91] | Wax Deposited % or Mass | 0.994 | 88 | Baltzer et al., Pedersen et al. compilation [50,54,55] |

Compounding this, many models draw on the same experimental datasets from the 1990s–2000s. Wax-weight studies repeatedly cite the Baltzer and Pedersen compilations [50,54,82], typically with eight or nine standard inputs (six carbon fractions $C_1$–$C_3$ … $C_{30+}$, oil specific gravity, system temperature, and occasionally pressure). On the

other hand, WDT studies rely on pressure and molar mass from a second recurring set (Daridon, Milhet, Ji, Metivaud and Robles [57–59,61–63]). There are 21 out of 41 studies drawn on just five shared datasets; only 16 use independent data. This creates an echo chamber effect (Table 10), where models are repeatedly tested on near-identical data. Because the same datasets are often reused for both tuning and evaluation, agreement between studies reflects shared data rather than independent confirmation.

**Table 10.** Reuse of shared source datasets across the reviewed studies.

| Dataset Sources | Main Target | Studies Reusing (n) | Models (n) | Studies |
|---|---|---|---|---|
| Baltzer et al., Pedersen et al. compilation (1991) [50,54,55] | Wax deposited %/mass | 9 | 20 | Kamari et al., 2013 [49]; Amar et al., 2022 [91]; Ahmadi, 2023 [108]; Ahmadi, 2025 [109]; Chu et al., 2017 [107]; Manshad et al., 2012 [55]; Eghtedaei et al., 2017 [81]; Gholami et al., 2018 [53]; Khalighi and Cheremisin, 2024 [67] |
| Daridon et al./Milhet et al./Ji et al./Metivaud et al./Robles et al. (1995–2005) [57–59,61,62] | WDT | 7 | 22 | Bian et al., 2019 [56]; Kamari et al., 2019 [60]; Moradi et al., 2013 [79]; Benamara et al., 2019 [88]; Amiri-Ramsheh et al., 2022 [93]; Mansourpoor et al., 2019 [89]; Amar et al., 2024 [117] |
| Wang (2010) [87] | Wax deposition rate | 4 | 11 | Xie and Xing, 2017 [66]; Xiao et al., 2022 [94]; Chen et al., 2024 [114]; Jin et al., 2025 [118] |
| Wei et al. (2010) [52] | Wax deposition rate | 3 | 5 | Wei et al., 2010 [52]; Kamari et al., 2014 [51]; Septiano et al., 2022 [64] |

### *5.3. Comparability of Error Metrics*

Cross-study comparison is further complicated by inconsistent, scale-dependent reporting. AAPRE is reported for only about two-thirds of the models (73 of 105). RMSE is reported more often, but it is scale-dependent (for example, <0.05 for wax thickness to 90–114 for wax solubility). As shown in Figure 9, RMSE cannot be compared across targets; hence, it is meaningful only within a single target. This leaves $R^2$ and AAPRE as the only metrics that transfer across targets. However, even these must be read together, because a high $R^2$ does not guarantee a low error.

This matters most for the wax deposited %/mass target. As shown in Figure 11, these models reach a median $R^2$ of 0.944 but a median AAPRE of about 20%. That is an order of magnitude worse than the deposition-rate target, which achieves a comparable $R^2$ at only 2.7% AAPRE. A model can therefore look excellent by $R^2$ yet be unfit for quantitative use.

The reason lies in how AAPRE is scaled. Because it is weighted inversely by the measured value (Equation (6)), the same absolute error looks very different across targets. WDT predictions (245–325 K [57–59,61–63]) show high RMSE but low AAPRE, whereas wax-weight predictions (mean ≈ 3%, range 0–13% [50,54,82]) show the reverse. $R^2$ and AAPRE are therefore the more transferable metrics, and future studies should report $R^2$, AAPRE, dataset size, and the validation protocol together.

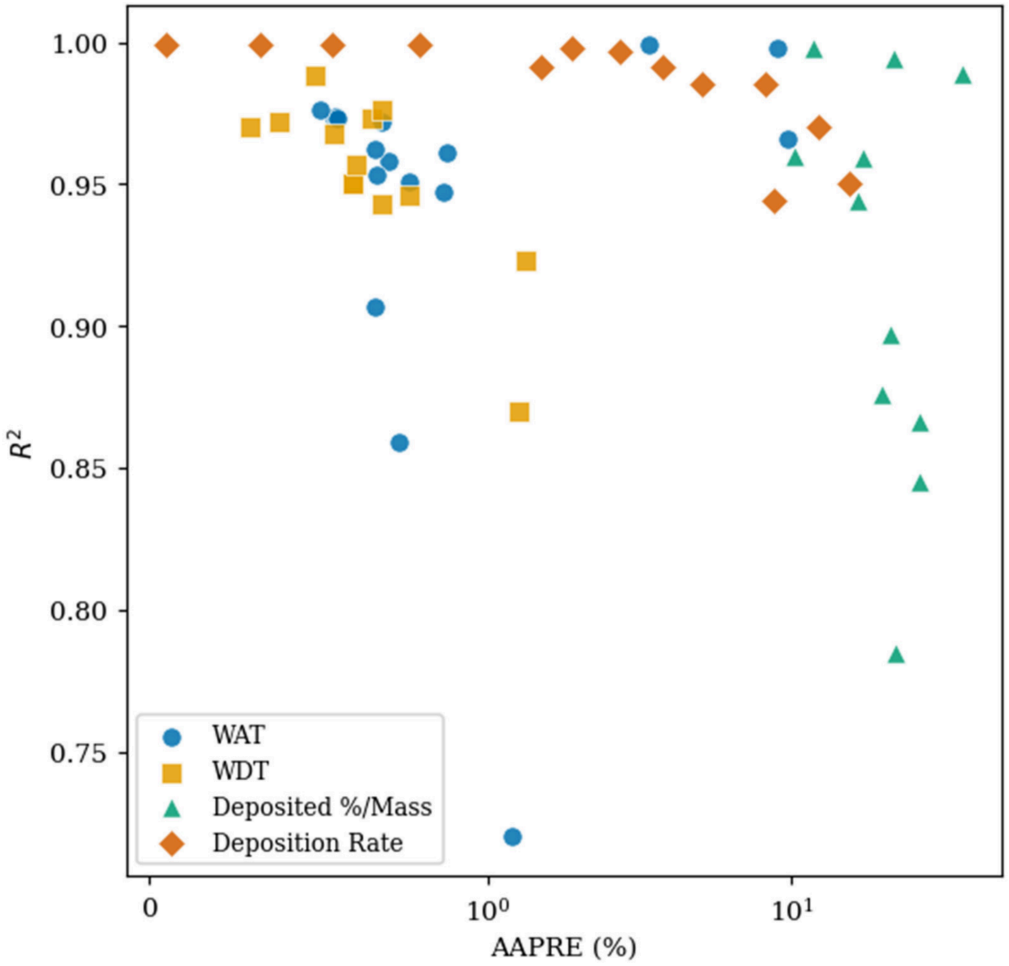


**Figure 11.** Reported $R^2$ versus AAPRE for the reviewed models, by prediction target, showing that a high $R^2$ does not guarantee a low percentage error.

### *5.4. Underused Feature Selection*

Feature selection remains underutilized despite consistent evidence of its value. Khalighi and Cheremisin [67] raised $R^2$ from 0.939 to 0.988 simply by removing two low-relevance inputs ($C_1$–$C_3$ and specific gravity) using Pearson's coefficient, identifying temperature, $C_8$–$C_{15}$, and $C_{16}$–$C_{22}$ as the dominant features. This is consistent with the sensitivity analysis of Manshad et al. [55] and supported by Ahmadi [108]. Xie and Xing [66] used gray relational analysis to retain viscosity, wall shear stress, temperature gradient, and the wall-wax crystal solubility coefficient. Bian et al. [56] established pressure and molar mass for WDT as the highest impact predictors, while Benamara et al. [90] and Amiri-Ramsheh et al. [95] highlighted pour and freezing points.

Therefore, systematic feature selection, such as sensitivity analysis, SHAP, mutual information, and PCA, should be performed, as they could reduce model complexity while improving interpretability and generalization [121,122].

Finally, Table 11 summarizes the recommended models for each prediction target.

While Table 11 provides a broad summary of the models applied to different wax-prediction targets, their reported performance cannot be directly compared because the studies frequently use different datasets, sample sizes, input variables, target scales, and validation procedures. Therefore, a more objective model-selection framework is provided in Table 12. The recommendations are based on three criteria: (1) direct comparative performance, with preference given to models evaluated against alternatives using the same dataset and validation procedure; (2) consistency of competitive performance across

multiple studies or datasets, where such evidence is available; and (3) suitability of the model architecture for the characteristics of the prediction problem and available data. Performance metrics obtained from different datasets or validation procedures are not used to directly rank the models.

**Table 11.** A summary of the recommended AI-based models used for wax deposition prediction in this review.

| Target | Input Parameters | Recommended Models |
| --- | --- | --- |
| WAT | Density, viscosity, pour point, freezing point, wax content; pressure, paraffin content, lumped fractions | LSSVM [68]; deep MLP-Adam [100]; XGBoost [112]; MLP-BR [90]; CatBoost-PSO [110] |
| WDT | Pressure, molar mass [57–59,61–63] | LSSVM or SVM-GWO [56,60]; MLP-LMA [60,105]; RBFNN-GA or RBFNN-ABC [88]; ANFIS-PSO [56]; GMDH or DT [88]; GEP [117] |
| Wax deposited %/mass | $C_1$–$C_3$, $C_4$–$C_7$, $C_8$–$C_{15}$, $C_{16}$–$C_{22}$, $C_{23}$–$C_{29}$, $C_{30+}$, specific gravity, temperature, pressure [50,54,82] | SVR or LSSVM or LSSVM-GA [49,53]; MLP-LMA or MLP-BR [53,55,91]; ANFIS-PSO, FIS-GA or HFGA [107,108]; CM-GA [90]; Gradient Boosting (XGBoost) emerging but lower-scoring on this target [109]; RBFNN-LMA [81] |
| | American Petroleum Institute Gravity (°API), pour point | MLP-LMA or MLP-BFGS [95]; GPNN [95] |
| | Temperature differential, flow rate, residence time | MLP-LMA [78] |
| Wax deposition rate | Wall shear stress, viscosity, temperature gradient at pipeline wall, wax concentration gradient | RBFNN [99]; stacked RF/XGBoost/SVR ensemble [72]; ENN-IRSA [114]; RF [73] |
| | Reynolds number, residual time, temperature driving force, wax content | ANFIS [105] |
| Wax solubility | Critical temperature of wax, temperature, pressure, critical temperature of gas system | Extra-trees or MLP-LMA [101] |
| Wax Thickness | Reynolds number, residence time, temperature driving force, wax content | MLP-LMA [83], ANFIS [105] |

It is worth mentioning that the practical implementation of AI-based wax deposition models depends strongly on the availability of their input variables under field operating conditions. Although laboratory datasets may contain detailed crude oil compositional information that can improve model accuracy, such information is not necessarily available at the frequency required for real-time prediction. In contrast, variables such as temperature, pressure, flow rate, viscosity, shear stress, density, pour point, and other routinely monitored process parameters can generally be obtained continuously through conventional field instrumentation and process monitoring systems. Consequently, AI models relying primarily on continuously measurable operational variables have greater potential for real-time or near-real-time implementation. Also, these parameters can partially reflect changes in the oil composition.

Therefore, the distinction between predictive accuracy and operational feasibility should be considered when evaluating AI models for field deployment. Models developed using detailed compositional information may demonstrate high accuracy on laboratory datasets but may require periodic compositional measurements rather than continuous monitoring.

**Table 12.** Model-selection guidance for AI-based wax prediction.

| Prediction Target | Input Characteristics | Recommended Starting Model(s) | Justification |
|---|---|---|---|
| Wax deposited %/mass | Compositional and operating variables; small tabular datasets | MLP or LSSVM; | MLP and LSSVM are repeatedly the strongest on the shared wax-weight datasets. |
| Wax deposition rate | Operational/flow variables | LSSVM, RF, or gradient boosting (XGBoost/ CatBoost) | CatBoost with nested/external validation [110] is the most robustly evaluated. LSSVM's near-perfect $R^2$ comes from a single small (n = 81) split and should be read with caution. |
| WDT | Pressure and molar mass | DT/RF or LSSVM | Tree models outperform NN/ANFIS alternatives in direct comparisons; LSSVM is repeatedly competitive. |
| WAT | Density, wax content, pour point and related variables | LSSVM or XGBoost | Best-performing models in direct within-study comparisons. |
| Wax solubility | Critical temperature of wax, temperature, pressure, critical temperature of gas system | MLP | MLP outperformed extra-trees in the available direct comparison. |
| Wax thickness | Reynolds number, residence time, temperature driving force, wax content | MLP | ANN outperformed ANFIS in the available comparison; however, evidence is limited to three studies. |

A practical implementation strategy could involve a hybrid approach in which periodically obtained compositional information is used to calibrate or update the AI model, while continuously measured operational variables are used for real-time prediction.

## 6. Conclusions and Way Forward

This review examined artificial intelligence approaches to wax deposition prediction in oil pipelines, organizing 41 primary studies into five model families and comparing their reported accuracy on target-stratified metrics. Across the field, MLP, SVM/LSSVM, neuro-fuzzy, and, most recently, tree-based models all achieve $R^2$ values frequently above 0.95. Tree-based gradient boosting is the most frequent winner in within-study head-to-head comparisons. However, its lead is target-dependent, so no single family can be declared universally superior.

Three issues nonetheless constrain progress. First, the field depends on a small pool of recycled 1990s–2000s datasets, creating an echo chamber that inflates apparent consensus. Second, the routinely reported near-perfect accuracies are obtained on very small datasets (a median of 98 points per study) with weak validation, so they likely overstate real-world generalization. Third, inconsistent, scale-dependent metric reporting, particularly of RMSE, prevents fair cross-study comparison. A high $R^2$ can still conceal a large AAPRE error. Two secondary patterns reinforce these: (1) optimizer selection is driven by convention rather than evidence, with no consistent ranking among LMA, BR, and BFGS, and (2) systematic feature selection remains underused despite clear gains when applied.

### *6.1. Limitations of This Review*

This review has several limitations. The systematic search relied on open bibliographic databases (OpenAlex and Semantic Scholar) supplemented by hand-searching, as subscription access to Scopus and Web of Science was unavailable. The scope was restricted to

peer-reviewed, English-language primary studies, so the gray literature was excluded, and seventeen otherwise-eligible reports could not be retrieved in full text.

In addition, the performance metrics analyzed are those reported by the original authors, which could not be independently verified. Because most studies use small, frequently reused datasets and a single train–test split, these values likely represent upper bounds on true performance rather than field-realistic accuracy. Finally, metrics from different studies are not directly comparable, as they come from different datasets, units, and validation protocols. This was mitigated by analyzing each prediction target separately and by limiting performance claims to within-study or same-dataset comparisons, but some incomparability across the pooled statistics remains.

### 6.2. Future Directions and Recommendations

Several concrete steps would strengthen the field. First, reporting should be standardized to include $R^2$, AAPRE, dataset size, and the validation protocol together, so that studies can be compared meaningfully.

Second, validation must become more rigorous. At present, 32 of the 41 studies rely on a single train–test split, 6 add k-fold cross-validation, and only 3 use external validation on independent data, with just one (Rifat et al. [110]) applying nested cross-validation, bootstrapping, and external testing. Validation should therefore move beyond single splits toward nested cross-validation and external testing across crude types, pressure regimes, and geographies.

Third, the field needs new experimental data. Progress is currently bounded by a handful of reused legacy datasets, so generating fresh measurements across different crude types, compositions, and operating conditions is the most direct way to break the echo chamber. New studies should also evaluate their models on the established legacy datasets, so that results on new data can be benchmarked against prior work.

Fourth, practical deployability deserves explicit attention. Models intended for real-time monitoring should favor field-measurable inputs such as temperature, viscosity, shear stress, density, and pour point over full laboratory compositional analysis. Future studies should therefore evaluate AI models using field-accessible variables, quantify the effect of reducing the number of input variables on predictive performance, and validate model robustness using long-term field data. Such efforts would facilitate the transition of AI-based wax deposition models from laboratory-scale predictive tools toward real-time flow-assurance monitoring and operational decision support. Studies should also report computational cost, training time, and inference speed, which are presently almost never stated. In addition, models should quantify predictive uncertainty rather than give point estimates alone. Uncertainty quantification is almost entirely absent, yet confidence intervals are what operational decisions such as pigging scheduling actually require.

Fifth, systematic feature selection such as sensitivity analysis, SHAP, mutual information, or PCA should become routine rather than incidental.

On the modeling side, gradient-boosting ensembles paired with SHAP are the most promising near-term option for the small tabular datasets typical of this problem, combining competitive accuracy with interpretability. Physics-informed and hybrid mechanistic–data-driven models, such as PINNs, are attractive for enforcing thermodynamic consistency and improving extrapolation, provided they are evaluated on out-of-distribution conditions and against physical-trend diagnostics rather than on in-sample accuracy alone. Data-centric strategies, such as generative augmentation, simulator-generated data, and transfer learning from abundant synthetic to scarce field data, directly target the data scarcity that ultimately bounds the field. Finally, for time-resolved deposition, sequence models (LSTM and attention-based architectures) coupled to real-time sensor streams could enable online,

adaptive prediction, moving wax modeling from static benchmarking toward operational flow-assurance systems. Together, these steps would move wax deposition modeling from static benchmarking on a handful of reused datasets toward reproducible, physically consistent and deployable flow-assurance tools.

**Author Contributions:** Conceptualization, Y.H., O.N. and E.A.E.; methodology, O.N. and E.H.L.T.; formal analysis, O.N. and E.H.L.T.; data curation, P.T.B.; validation, P.T.B., E.A.E., E.S. and M.S.H.; writing—original draft preparation, O.N. and E.H.L.T.; writing—review and editing, Y.H., E.S. and M.S.H.; supervision, Y.H.; project administration, Y.H.; funding acquisition, Y.H. and E.S. All authors have read and agreed to the published version of the manuscript.

**Funding:** This research was funded by Yayasan Universiti Teknologi PETRONAS YUTP-FRG, grant number (015LC0-533).

**Data Availability Statement:** No new data were created or analyzed in this study. Data sharing is not applicable to this article.

**Acknowledgments:** The authors would like to express their sincere gratitude to Universiti Teknologi PETRONAS (UTP).

**Conflicts of Interest:** The authors declare no conflicts of interest.

## References

1. Olah, G.A.; Molnár, Á. *Hydrocarbon Chemistry*; John Wiley & Sons: Hoboken, NJ, USA, 2003.
2. Ragunathan, T.; Husin, H.; Wood, C.D. Wax formation mechanisms, wax chemical inhibitors and factors affecting chemical inhibition. *Appl. Sci.* **2020**, *10*, 479. [CrossRef]
3. Srivastava, S.; Handoo, J.; Agrawal, K.; Joshi, G. Phase-transition studies in n-alkanes and petroleum-related waxes—A review. *J. Phys. Chem. Solids* **1993**, *54*, 639–670. [CrossRef]
4. Xie, Y.; Li, H.; Xu, M.; Su, Y.; Zhang, C.; Han, S.; Zhang, J. Effect of shear on durability of viscosity reduction of electrically-treated waxy crude oils. *Energy* **2023**, *284*, 128605. [CrossRef]
5. Theyab, M.A. Wax deposition process: Mechanisms, affecting factors and mitigation methods. *Open Access J. Sci.* **2018**, *2*, 112–118. [CrossRef]
6. Aiyejina, A.; Chakrabarti, D.P.; Pilgrim, A.; Sastry, M. Wax formation in oil pipelines: A critical review. *Int. J. Multiph. Flow* **2011**, *37*, 671–694. [CrossRef]
7. Zhu, H.; Lei, Y.; Yu, P.; Li, C.; Yang, F.; Yao, B.; Yang, S.; Peng, H. Wax deposition during the transportation of waxy crude oil: Mechanisms, influencing factors, modeling, and outlook. *Energy Fuels* **2024**, *38*, 9131–9152. [CrossRef]
8. Chen, W.; Zhang, X.; Zhao, Z.; Yin, C. UNIQUAC model for wax solution with pour point depressant. *Fluid Phase Equilibria* **2009**, *280*, 9–15. [CrossRef]
9. Zhang, C.; Gao, C.; Gao, F.; Wang, J.; Zhang, D.; Wang, Y.; Xu, D. Synthesis of comb bipolymers and their pour point depressing properties. *Pet. Sci.* **2014**, *11*, 155–160. [CrossRef]
10. Apte, M.S.; Matzain, A.; Zhang, H.-Q.; Volk, M.; Brill, J.P.; Creek, J.L. Investigation of paraffin deposition during multiphase flow in pipelines and wellbores—Part 2: Modeling. *J. Energy Resour. Technol.* **2001**, *123*, 150–157. [CrossRef]
11. Burger, E.; Perkins, T.; Striegler, J. Studies of wax deposition in the trans Alaska pipeline. *J. Pet. Technol.* **1981**, *33*, 1075–1086. [CrossRef]
12. Hernandez, O.; Hensley, H.; Sarica, C.; Brill, J.; Volk, M.; Delle-Case, E. Improvements in single-phase paraffin deposition modeling. *SPE Prod. Facil.* **2004**, *19*, 237–244. [CrossRef]
13. Singh, P.; Venkatesan, R.; Fogler, H.S.; Nagarajan, N. Formation and aging of incipient thin film wax-oil gels. *AIChE J.* **2000**, *46*, 1059–1074. [CrossRef]
14. Wang, W.; Huang, Q.; Wang, C.; Li, S.; Qu, W.; Zhao, J.; He, M. Effect of operating conditions on wax deposition in a laboratory flow loop characterized with DSC technique. *J. Therm. Anal. Calorim.* **2015**, *119*, 471–485. [CrossRef]
15. Sousa, A.; Matos, H.; Guerreiro, L. Preventing and removing wax deposition inside vertical wells: A review. *J. Pet. Explor. Prod. Technol.* **2019**, *9*, 2091–2107. [CrossRef]
16. Li, B.; Guo, Z.; Zheng, L.; Shi, E.; Qi, B. A comprehensive review of wax deposition in crude oil systems: Mechanisms, influencing factors, prediction and inhibition techniques. *Fuel* **2024**, *357*, 129676. [CrossRef]
17. Rittirong, A. *Paraffin Deposition Under Two-Phase Gas-Oil Slug Flow in Horizontal Pipes*; The University of Tulsa: Tulsa, OK, USA, 2014.

18. Rittirong, A.; Panacharoensawad, E.; Sarica, C. Experimental study of paraffin deposition under two-phase gas/oil slug flow in horizontal pipes. *SPE Prod. Oper.* **2017**, *32*, 99–117. [CrossRef]
19. Zhuang, Q.; Li, H.; Bao, Y.; Liu, G.; Liu, D. Research on the prediction model of wax deposition thickness of waxy crude oil in pipeline transportation. *Pet. Sci. Technol.* **2024**, *42*, 869–885. [CrossRef]
20. Quan, Q.; Ran, W.; Yang, L.; Gao, G.; Wang, S.; Gong, J. The effect of pressure on wax deposition from wax-solvent mixtures with natural gas. *J. Pet. Sci. Eng.* **2018**, *171*, 1318–1325. [CrossRef]
21. Chen, Y.; Jing, J.; Sun, J.; Wang, K.; Wang, S. Progress and perspectives of wax deposition in oil-gas systems: A review. *Chem. Eng. Res. Des.* **2024**, *208*, 348–358. [CrossRef]
22. Fung, G.; Backhaus, W.; McDaniel, S.; Erdogmus, M. To pig or not to pig: The marlin experience with stuck pig. In *Offshore Technology Conference*; OnePetro: Richardson, TX, USA, 2006; p. OTC-18387-MS.
23. Beiny, D.; Mullin, J.; Lewtas, K. Crystallization of n-dotriacontane from hydrocarbon solution with polymeric additives. *J. Cryst. Growth* **1990**, *102*, 801–806. [CrossRef]
24. Duan, J.; Liu, H.; Guan, J.; Hua, W.; Jiao, G.; Gong, J. Wax deposition modeling of oil/gas stratified smooth pipe flow. *AIChE J.* **2016**, *62*, 2550–2562. [CrossRef]
25. Ghanaei, E.; Esmaeilzadeh, F.; Fathikalajahi, J. Wax formation from paraffinic mixtures: A simplified thermodynamic model based on sensitivity analysis together with a new modified predictive UNIQUAC. *Fuel* **2012**, *99*, 235–244. [CrossRef]
26. Lei, Y.; Wang, H.; Li, S.-S.; Liu, X.-Q.; Zhu, H.-R.; Gao, Y.-M.; Peng, H.-P.; Yu, P.-F. Effect of existence state of asphaltenes on the asphaltenes-wax interaction in wax deposition. *Pet. Sci.* **2023**, *20*, 507–514. [CrossRef]
27. Yan, M.; Li, G.; Li, X. Study on the effect of crude oil composition on waxing characteristics of waxy crude oil. *IOP Conf. Ser. Mater. Sci. Eng.* **2018**, *452*, 032018. [CrossRef]
28. Baashar, Y.; Hamed, Y.; Alkawsi, G.; Capretz, L.F.; Alhussian, H.; Alwadain, A.; Al-Amri, R. Evaluation of postgraduate academic performance using artificial intelligence models. *Alex. Eng. J.* **2022**, *61*, 9867–9878. [CrossRef]
29. Géron, A. *Hands-on Machine Learning with Scikit-Learn, Keras, and TensorFlow*; O'Reilly Media, Inc.: Sebastopol, CA, USA, 2022.
30. Hamed, Y.; Abd Rahman, M.S.; Ab Kadir, M.Z.A.; Osman, M.; Ariffin, A.M.; Ab Aziz, N.F. Artificial intelligence forecasting for transmission line ampacity. In *Towards Intelligent Systems Modeling and Simulation: With Applications to Energy, Epidemiology and Risk Assessment*; Springer: Berlin/Heidelberg, Germany, 2021; pp. 217–234.
31. Haykin, S. *Neural Networks and Learning Machines, 3/E*; Pearson Education India: Bengaluru, India, 2009.
32. Ahsan, M.M.; Mahmud, M.P.; Saha, P.K.; Gupta, K.D.; Siddique, Z. Effect of data scaling methods on machine learning algorithms and model performance. *Technologies* **2021**, *9*, 52. [CrossRef]
33. Guido, R.; Ferrisi, S.; Lofaro, D.; Conforti, D. An overview on the advancements of support vector machine models in healthcare applications: A review. *Information* **2024**, *15*, 235. [CrossRef]
34. Rivas-Perea, P.; Cota-Ruiz, J.; Chaparro, D.G.; Venzor, J.A.P.; Carreón, A.Q.; Rosiles, J.G. Support vector machines for regression: A succinct review of large-scale and linear programming formulations. *Int. J. Intell. Sci.* **2013**, *3*, 5–14.
35. Yu, J.; Spiliopoulos, K. Normalization effects on deep neural networks. *arXiv* **2022**, arXiv:2209.01018.
36. Yu, T.; Zhu, H. Hyper-parameter optimization: A review of algorithms and applications. *arXiv* **2020**, arXiv:2003.05689.
37. Cortes, C.; Vapnik, V. Support-vector networks. *Mach. Learn.* **1995**, *20*, 273–297. [CrossRef]
38. Vapnik, V. *The Nature of Statistical Learning Theory*; Springer Science & Business Media: Berlin/Heidelberg, Germany, 2013.
39. Hamed, Y.; Alzahrani, A.I.; Shafie, A.F.; Mustaffa, Z.; Ismail, M.C.; Eng, K.K. Two steps hybrid calibration algorithm of support vector regression and K-nearest neighbors. *Alex. Eng. J.* **2020**, *59*, 1181–1190. [CrossRef]
40. Suykens, J.A.K.; Vandewalle, J. Least Squares Support Vector Machine Classifiers. *Neural Process. Lett.* **1999**, *9*, 293–300. [CrossRef]
41. Van Gestel, T.; De Brabanter, J.; De Moor, B.; Vandewalle, J.; Suykens, J.; Van Gestel, T. Least squares support vector machines. In *Least Squares Support Vector Machines*; World Scientific: Singapore, 2002; Volume 4.
42. Specht, D.F. A general regression neural network. *IEEE Trans. Neural Netw.* **1991**, *2*, 568–576. [CrossRef] [PubMed]
43. Warsito, B.; Santoso, R.; Suparti; Yasin, H. Cascade forward neural network for time series prediction. *J. Phys. Conf. Ser.* **2018**, *1025*, 012097.
44. Mamdani, E.H.; Assilian, S. An experiment in linguistic synthesis with a fuzzy logic controller. *Int. J. Hum.-Comput. Stud.* **1999**, *51*, 135–214. [CrossRef]
45. Zadeh, L.A. Fuzzy sets. *Inf. Control* **1965**, *8*, 338–353. [CrossRef]
46. Abraham, A. Adaptation of fuzzy inference system using neural learning. In *Fuzzy Systems Engineering: Theory and Practice*; Springer: Berlin/Heidelberg, Germany, 2005; pp. 53–83.
47. Jang, J.-S. ANFIS: Adaptive-network-based fuzzy inference system. *IEEE Trans. Syst. Man. Cybern.* **1993**, *23*, 665–685. [CrossRef]
48. Takagi, T.; Sugeno, M. Fuzzy identification of systems and its applications to modeling and control. *IEEE Trans. Syst. Man Cybern.* **1985**, *SMC-15*, 116–132. [CrossRef]
49. Kamari, A.; Khaksar-Manshad, A.; Gharagheizi, F.; Mohammadi, A.H.; Ashoori, S. A Robust Model for Determination of Wax Deposition in Oil Systems. *Ind. Eng. Chem. Res.* **2013**, *52*, 15664–15672. [CrossRef]

50. Pedersen, W.B.; Baltzer Hansen, A.; Larsen, E.; Nielsen, A.B.; Roenningsen, H.P. Wax precipitation from North Sea crude oils. 2. Solid-phase content as function of temperature determined by pulsed NMR. *Energy Fuels* **1991**, *5*, 908–913. [CrossRef]
51. Kamari, A.; Mohammadi, A.H.; Bahadori, A.; Zendehboudi, S. A Reliable Model for Estimating the Wax Deposition Rate During Crude Oil Production and Processing. *Pet. Sci. Technol.* **2014**, *32*, 2837–2844. [CrossRef]
52. Wei, Y.; Wu, M.; Ling, Z. *Wax Deposition Rate Model for Crude Oil Pipeline Based on Neural Network*; IEEE: Piscataway, NJ, USA, 2010; Volume 10, pp. 760–762.
53. Gholami, A.; Ansari, H.R.; Ahmadi, S. Combining of intelligent models through committee machine for estimation of wax deposition. *J. Chin. Chem. Soc.* **2018**, *65*, 925–931. [CrossRef]
54. Hansen, A.B.; Larsen, E.; Pedersen, W.B.; Nielsen, A.B.; Roenningsen, H.P. Wax precipitation from North Sea crude oils. 3. Precipitation and dissolution of wax studied by differential scanning calorimetry. *Energy Fuels* **1991**, *5*, 914–923. [CrossRef]
55. Manshad, A.K.; Ashoori, S.; Manshad, M.K.; Omidvar, P. The prediction of wax precipitation by neural network and genetic algorithm and comparison with a multisolid model in crude oil systems. *Pet. Sci. Technol.* **2012**, *30*, 1369–1378. [CrossRef]
56. Bian, X.Q.; Huang, J.H.; Wang, Y.; Liu, Y.B.; Kaushika Kasthuriarachchi, D.T.; Huang, L.J. Prediction of Wax Disappearance Temperature by Intelligent Models. *Energy Fuels* **2019**, *33*, 2934–2949. [CrossRef]
57. Ji, H.-Y.; Tohidi, B.; Danesh, A.; Todd, A.C. Wax phase equilibria: Developing a thermodynamic model using a systematic approach. *Fluid Phase Equilibria* **2004**, *216*, 201–217. [CrossRef]
58. Daridon, J.L.; Pauly, J.; Milhet, M. High pressure solid–liquid phase equilibria in synthetic waxes. *Phys. Chem. Chem. Phys.* **2002**, *4*, 4458–4461. [CrossRef]
59. Milhet, M.; Pauly, J.; Coutinho, J.A.P.; Dirand, M.; Daridon, J.L. Liquid–solid equilibria under high pressure of tetradecane+pentadecane and tetradecane+hexadecane binary systems. *Fluid Phase Equilibria* **2005**, *235*, 173–181. [CrossRef]
60. Kamari, A.; Rahimzadeh, A.; Mohammadi, A.H.; Ramjugernath, D. Evaluation of wax disappearance temperatures in hydrocarbon fluids using soft computing approaches. *Pet. Sci. Technol.* **2019**, *37*, 829–836. [CrossRef]
61. Robles, L.; Espeau, P.; Mondieig, D.; Haget, Y.; Oonk, H.A.J. Polymorphisme et alliages moleculaires dans le systeme C17H36-C19H40. *Thermochim. Acta* **1996**, *274*, 61–72. [CrossRef]
62. Metivaud, V.; Rajabalee, F.; Oonk, H.A.; Mondieig, D.; Haget, Y. Complete determination of the solid (RI)-liquid equilibria of four consecutive n-alkane ternary systems in the range C14H30-C21H44 using only binary data. *Can. J. Chem.* **1999**, *77*, 332–339. [CrossRef]
63. Vafaie-Sefti, M.; Mousavi-Dehghani, S.A.; Mohammad-Zadeh Bahar, M. Modification of multisolid phase model for prediction of wax precipitation: A new and effective solution method. *Fluid Phase Equilibria* **2000**, *173*, 65–80. [CrossRef]
64. Septiano, J.; Yasutra, A.; Rahmawati, S.D. Build of Machine Learning Proxy Model for Prediction of Wax Deposition Rate in Two Phase Flow Water-Oil. *Sci. Contrib. Oil Gas.* **2022**, *45*, 53–67. [CrossRef]
65. Fan, K.; Huang, Q.; Li, S.; Yu, W. The wax deposition rate of water-in-crude oil emulsions based on the laboratory flow loop experiment. *J. Dispers. Sci. Technol.* **2017**, *38*, 8–18. [CrossRef]
66. Xie, Y.; Xing, Y. A prediction method for the wax deposition rate based on a radial basis function neural network. *Petroleum* **2017**, *3*, 237–241. [CrossRef]
67. Khalighi, J.; Cheremisin, A. Wax precipitation prediction using a novel intelligent method: Modeling and data analysis. *Pet. Sci. Technol.* **2024**, *42*, 846–868.
68. Kouhi, M.M.; Shafiei, A.; Bekkuzhina, T.; Abutalip, M. New intelligent models for predicting wax appearance temperature using experimental data–Flow assurance implications. *Fuel* **2025**, *380*, 133146. [CrossRef]
69. Zhang, Y.; Gong, J.; Wu, H. An Experimental Study on Wax Deposition of Water in Waxy Crude Oil Emulsions. *Pet. Sci. Technol.* **2010**, *28*, 1653–1664. [CrossRef]
70. Hoffmann, R.; Amundsen, L. Single-Phase Wax Deposition Experiments. *Energy Fuels* **2009**, *24*, 1069–1080. [CrossRef]
71. Quan, Q.; Gong, J.; Wang, W.; Wang, P. The Influence of Operating Temperatures on Wax Deposition During Cold Flow and Hot Flow of Crude Oil. *Pet. Sci. Technol.* **2015**, *33*, 272–277. [CrossRef]
72. Gao, Y.; Luo, Z.; Guo, J. A WGAN-GP and stacking ensemble-based framework for enhanced prediction of wax deposition rate in crude oil pipelines. *Sci. Rep.* **2026**, *16*, 19989. [CrossRef] [PubMed]
73. Sarkodie, K.; Agyepong, J.; Agyei, E.; Arkoh, G.; Arhin, R.; Ankomah, F.; Adenutsi, C.D.; Erzuah, S. Machine learning-based surrogate correlation for prediction of wax deposition rate in oil and gas pipelines. *Petroleum* **2026**, *12*, 350–365. [CrossRef]
74. Wang, W.; Huang, Q. Prediction for wax deposition in oil pipelines validated by field pigging. *J. Energy Inst.* **2014**, *87*, 196–207. [CrossRef]
75. Yao, B.; Zhao, D.; Zhang, Z.; Huang, C. Safety study on wax deposition in crude oil pipeline. *Processes* **2021**, *9*, 1572. [CrossRef]
76. Huang, Q.; Ma, J. Prediction of wax deposition of crude using statistical and neural network methods. In *International Pipeline Conference*; ASME: New York, NY, USA, 2008; Volume 48609, pp. 341–345.
77. Obanijesu, E.O.; Omidiora, E.O. Artificial neural network's prediction of wax deposition potential of Nigerian crude oil for pipeline safety. *Pet. Sci. Technol.* **2008**, *26*, 1977–1991. [CrossRef]

78. Kelechukwu, E.M.; Al-Salim, H.S.; Saadi, A. Prediction of wax deposition problems of hydrocarbon production system. *J. Pet. Sci. Eng.* **2013**, *108*, 128–136. [CrossRef]
79. Moradi, G.; Mohadesi, M.; Moradi, M.R. Prediction of wax disappearance temperature using artificial neural networks. *Pet. Sci. Eng.* **2013**, *108*, 74–81. [CrossRef]
80. Behbahani, T.J.; Beigi, A.A.M.; Taheri, Z.; Ghanbari, B. Investigation of wax precipitation in crude oil: Experimental and modeling. *Petroleum* **2015**, *1*, 223–230. [CrossRef]
81. Eghtedaei, R.; Sasanipour, J.; Zarrabi, H.; Palizian, M.; Baghban, A. Estimation of wax deposition in the oil production units using RBF-ANN strategy. *Pet. Sci. Technol.* **2017**, *35*, 1737–1742. [CrossRef]
82. Pedersen, K.S.; Skovborg, P.; Roenningsen, H.P. Wax precipitation from North Sea crude oils. 4. Thermodynamic modeling. *Energy Fuels* **1991**, *5*, 924–932. [CrossRef]
83. Saeedi Dehaghani, A.H. An intelligent model for predicting wax deposition thickness during turbulent flow of oil. *Pet. Sci. Technol.* **2017**, *35*, 1706–1711. [CrossRef]
84. Lund, H.J. Investigation of Paraffin Deposition During Single Phase Flow in Pipelines. Ph.D. Thesis, University of TULSA, Tulsa, OK, USA, 1998.
85. Venkatesan, R. *The Deposition and Rheology of Organic Gels*; The University of Michigan: Ann Arbor, MI, USA, 2004.
86. Hernandez, O.C. Investigation of Single-Phase Paraffin Deposition Characteristics. Master's Thesis, The University of Tulsa, Tulsa, OK, USA, 2002.
87. Wang, X.L. *The Wax Deposition Phenomena Prediction of Huachi Oil Pipelines*; Xi'an Shiyou University: Xi'an, China, 2010.
88. Benamara, C.; Nait Amar, M.; Gharbi, K.; Hamada, B. Modeling Wax Disappearance Temperature Using Advanced Intelligent Frameworks. *Energy Fuels* **2019**, *33*, 10959–10968. [CrossRef]
89. Mansourpoor, M.; Azin, R.; Osfouri, S.; Izadpanah, A. Experimental measurement and modeling study for estimation of wax disappearance temperature. *J. Dispers. Sci. Technol.* **2019**, *40*, 161–170. [CrossRef]
90. Benamara, C.; Gharbi, K.; Nait Amar, M.; Hamada, B. Prediction of Wax Appearance Temperature Using Artificial Intelligent Techniques. *Arab. J. Sci. Eng.* **2020**, *45*, 1319–1330. [CrossRef]
91. Amar, M.N.; Jahanbani Ghahfarokhi, A.; Shang Wui Ng, C. Predicting wax deposition using robust machine learning techniques. *Petroleum* **2022**, *8*, 167–173. [CrossRef]
92. Askari, M.; Taheri, A.; Kochakpour, J.; Sasanpour, M.T. An intelligent gamma-ray technique for determining wax thickness in pipelines. *Appl. Radiat. Isot.* **2021**, *172*, 109667. [CrossRef] [PubMed]
93. Amiri-Ramsheh, B.; Safaei-Farouji, M.; Larestani, A.; Zabihi, R.; Hemmati-Sarapardeh, A. Modeling of wax disappearance temperature (WDT) using soft computing approaches: Tree-based models and hybrid models. *J. Pet. Sci. Eng.* **2022**, *208*, 109774. [CrossRef]
94. Xiao, R.; Jin, S. Prediction model of wax deposition rate based on woabpnn algorithm. *Front. Heat Mass Transf.* **2022**, *18*, 1–7. [CrossRef]
95. Amiri-Ramsheh, B.; Zabihi, R.; Hemmati-Sarapardeh, A. Modeling wax deposition of crude oils using cascade forward and generalized regression neural networks: Application to crude oil production. *Geoenergy Sci. Eng.* **2023**, *224*, 211613. [CrossRef]
96. Roenningsen, H.P.; Bjoerndal, B.; Baltzer Hansen, A.; Batsberg Pedersen, W. Wax precipitation from North Sea crude oils: 1. Crystallization and dissolution temperatures, and Newtonian and non-Newtonian flow properties. *Energy Fuels* **1991**, *5*, 895–908. [CrossRef]
97. Lira-Galeana, C.; Firoozabadi, A.; Prausnitz, J.M. Thermodynamics of wax precipitation in petroleum mixtures. *AIChE J.* **1996**, *42*, 239–248. [CrossRef]
98. Elsharkawy, A.M.; Al-Sahhaf, T.A.; Fahim, M.A. Wax deposition from Middle East crudes. *Fuel* **2000**, *79*, 1047–1055. [CrossRef]
99. Sultana, F.; Abdallah, E.M.; Dong, S.; Mukhtar, Y.M.F. Development of Predictive Model for Wax Formation in Deep-water Pipeline Using Machine learning. *J. Phys. Conf. Ser.* **2023**, *2594*, 012042.
100. Aguilar-Hernández, M.; Sheremetov, L.; Ortega-Rodríguez, A. Predicting wax formation in High-Pressure conditions for condensate samples using Machine learning. *Fuel* **2025**, *394*, 135183. [CrossRef]
101. Youcefi, M.R.; Alatefi, S.; Nait Amar, M.; Alkouh, A. Data-driven modeling of wax solubility in supercritical carbon dioxide and ethane systems. *J. Supercrit. Fluids* **2026**, *230*, 106867. [CrossRef]
102. Mohammadi, A.H.; Eslamimanesh, A.; Richon, D. Wax Solubility in Gaseous System: Thermodynamic Consistency Test of Experimental Data. *Ind. Eng. Chem. Res.* **2011**, *50*, 4731–4740. [CrossRef]
103. Mohammadi, A.H.; Gharagheizi, F.; Eslamimanesh, A.; Richon, D. Evaluation of experimental data for wax and diamondoids solubility in gaseous systems. *Chem. Eng. Sci.* **2012**, *81*, 1–7. [CrossRef]
104. Kondori, J.; Hashemi, H.; Babaee, S.; Javanmardi, J.; Mohammadi, A.H.; Ramjugernath, D. A thermodynamic consistency test for experimental isobaric data of wax solubility in gaseous systems. *Fluid Phase Equilibria* **2015**, *388*, 182–187. [CrossRef]
105. Jalalnezhad, M.J.; Kamali, V. Development of an intelligent model for wax deposition in oil pipeline. *J. Pet. Explor. Prod. Technol.* **2016**, *6*, 129–133. [CrossRef]
106. Rosvold, K. Wax Deposition Models. Master's Thesis, Norwegian University of Science and Technology, Trondheim, Norway, 2008.

107. Chu, Z.Q.; Sasanipour, J.; Saeedi, M.; Baghban, A.; Mansoori, H. Modeling of wax deposition produced in the pipelines using PSO-ANFIS approach. *Pet. Sci. Technol.* **2017**, *35*, 1974–1981. [CrossRef]
108. Ahmadi, M. Data-driven approaches for predicting wax deposition. *Energy* **2023**, *265*, 126296. [CrossRef]
109. Ahmadi, M. From composition to deposition: A machine learning framework for wax deposition prediction in petroleum fluids using compositional properties. *Phys. Fluids* **2025**, *37*, 072132. [CrossRef]
110. Rifat, H.R.; Abduljabbar, A.; Mohyaldinna, M.E. Categorical Boosting-PSO: A SHAP-Interpretable Hybrid Framework for High-Fidelity Wax Appearance Temperature Prediction in Subsea Pipelines. *Eng. Rep.* **2026**, *8*, e70979. [CrossRef]
111. Alcazar-Vara, L.A.; Buenrostro-Gonzalez, E. Characterization of the wax precipitation in Mexican crude oils. *Fuel Process. Technol.* **2011**, *92*, 2366–2374. [CrossRef]
112. Yadav, A.; Karamti, H.; Sur, D.; Menon, S.V.; Issa, B.S.; Shit, D.; Sunitha, S.; Panigrahi, R. Toward accurate modeling of wax appearance temperature (WAT) using intelligent ensemble techniques: Application to heavy crude oil production. *Chem. Eng. Sci.* **2025**, *319*, 122296. [CrossRef]
113. Kim, J.H.; Han, S.L.; Seo, Y.J.; Moon, B.; Lee, Y.S. The development of an AI-based model to predict the location and amount of wax in oil pipelines. *J. Pet. Sci. Eng.* **2022**, *209*, 109813. [CrossRef]
114. Chen, Z.; Wang, N.; Jin, W.; Li, D. Prediction Model of Wax Deposition Rate in Waxy Crude Oil Pipelines by Elman Neural Network Based on Improved Reptile Search Algorithm. *Energy Eng.* **2024**, *121*, 1007–1026. [CrossRef]
115. Wang, X.L. Prediction and Analysis of Wax Deposition in Pipeline Crude Oil in Huachi Operation Area. Master's Thesis, Xi'an Shiyou University, Xi'an, China, 2010.
116. Yang, H.M. Study on Wax Deposition Law and Paraffin Inhibitor in Kenli Crude Oil Pipeline. Master's Thesis, Southwest Petroleum University, Chengdu, China, 2015.
117. Amar, M.N.; Zeraibi, N.; Benamara, C.; Djema, H.; Saifi, R.; Gareche, M. Modeling wax disappearance temperature using robust white-box machine learning. *Fuel* **2024**, *376*, 132703. [CrossRef]
118. Jin, W.; Chen, Z.; Dai, K.; Quan, Q.; Ren, Z. Prediction of Wax Deposition Rate of Waxy Crude Oil Based on Improved Elman Neural Network. *Processes* **2025**, *13*, 3315. [CrossRef]
119. Zheng, W.L. Study on Wax Deposition Model for Deep-Water High-Viscosity and High-Condensation Crude Oil Pipelines. Master's Thesis, Southwest Petroleum University, Chengdu, China, 2018.
120. Zhang, Y. Research on Wax Deposition Prediction Algorithm for Waxy Crude Oil Pipeline Based on Machine Learning. Master's Thesis, Northeast Petroleum University, Daqing, China, 2019.
121. Haq, I.U.; Lal, B. *Machine Learning in Wax Deposition*; Springer Nature: Cham, Switzerland, 2023; pp. 141–153.
122. Kraev, E.; Koseoglu, B.; Traverso, L.; Topiwalla, M. Shap-Select: Lightweight Feature Selection Using SHAP Values and Regression. *arXiv* **2024**, arXiv:2410.06815.


**Disclaimer/Publisher's Note:** The statements, opinions and data contained in all publications are solely those of the individual author(s) and contributor(s) and not of MDPI and/or the editor(s). MDPI and/or the editor(s) disclaim responsibility for any injury to people or property resulting from any ideas, methods, instructions or products referred to in the content.